Medizinische Fakultät
der
Universität Duisburg-Essen

Aus der Klinik für Neurologie

Analysis of microvascular remodeling after transient focal cerebral ischemia using light-sheet fluorescence microscopy

I n a u g u r a l d i s s e r t a t i o n
zur
Erlangung des Doktorgrades der Medizin
durch die Medizinische Fakultät
der Universität Duisburg-Essen

Vorgelegt von
Yachao Qi
aus China
2022

DOI: 10.17185/duepublico/81287
URN: urn:nbn:de:hbz:465-20231213-092113-9

Dekan: Herr Univ.-Prof. Dr. med. J. Buer
Gutachter/in: Herr Univ.-Prof. Dr. med. D. M. Hermann
Gutachter/in: Herr Prof. Dr. med. M. Frings

Tag der mündlichen Prüfung: 26. Oktober 2023

List of publications

Philippa, Spangenberg, Nina Hagemann, Anthony Squire, Nils Förster, Sascha D. Krauß, **Yachao Qi**, Ayan Mohamud Yusuf, Jing Wang, Anika Grüneboom, Lennart Kowitz, Sebastian Korste, Matthias Totzeck, Zülal Cibir, Ali Ata Tuz, Vikramjeet Singh, Devon Siemes, Laura Struensee, Daniel R. Engel, Peter Ludewig, Luiza Martins, Nascentes Melo, Iris Helfrich, Jianxu Chen, Matthias Gunzer, Dirk M. Hermann, Axel Mosig (Schroeter et al.). Rapid and fully automated blood vasculature analysis in 3D light-sheet image volumes of different organs. bioRxiv;
https://doi.org/10.1101/2022.09.14.507895

Jonas Gregorius, Chen Wang, Oumaima Stambouli, Tanja Hussner, **Yachao Qi**, Tobias Tertel, Verena Börger, Ayan Mohamud Yusuf, Nina Hagemann, Dongpei Yin, Robin Dittrich, Yanis Mouloud, Fabian D. Mairinger, Fouzi El Magraoui, Aurel Popa-Wagner, Christoph Kleinschnitz, Thorsten R. Doeppner, Matthias Gunzer, Helmut E. Meyer, Bernd Giebel, Dirk M. Hermann (2021). Small extracellular vesicles obtained from hypoxic mesenchymal stromal cells have unique characteristics that promote cerebral angiogenesis, brain remodeling, and neurological recovery after focal cerebral ischemia in mice. Basic research in cardiology 116:40
https://doi.org/10.1007/s00395-021-00881-9

Ayan Mohamud Yusuf, Nina Hagemann, Sarah Schulten, Olessja Rausch, Kristina Wagner, Tanja Hussner, **Yachao Qi**, Matthias Totzeck, Christoph Kleinschnitz, Anthony Squire, Matthias Gunzer and Dirk M. Hermann (2021). Light Sheet Microscopy Using FITC-Albumin Followed by Immunohistochemistry of the Same Rehydrated Brains Reveals Ischemic Brain Injury and Early Microvascular Remodeling. Front. Cell. Neurosci. 14:625513.
https://doi.org/10.3389/fncel.2020.625513

Maryam Sardari, Egor Dzyubenko, Ben Schmermund, Dongpei Yin, **Yachao Qi,** Christoph Kleinschnitz, and Dirk M. Hermann (2020). Dose-dependent microglial and

astrocytic responses associated with post-ischemic neuroprotection after lipopolysaccharide-induced sepsis in mice Front. Cell. Neurosci. 14:26. https://doi.org/10.3389/fncel.2020.00026

Contents

INTRODUCTION

1.1 Ischemic stroke

Ischemic stroke is the most prevalent cause of disability and the second leading cause of death, responsible for approximately 11% of all deaths worldwide in adult (Katan, et. al., 2018). It is clinically defined as a syndrome of acute focal neurological deficits caused by supplied arterial occlusion of the central nervous system. A wide range of risk factors may cause arterial occlusion (Murphy et al., 2020). Lumen-narrowing arteriosclerosis, cardioembolism, and arterio-arterial thromboembolism can trigger ischemic stroke. In particular, the obstruction of large arteries, such as the internal carotid and middle cerebral arteries, is associated with large brain infarcts. Due to the disruption of blood flow to the affected area, the delivery of oxygen and metabolic substrates to neurons is limited, which causes a reduction in ATP and energy-rich metabolites. These, in turn, lead to a series of alterations in ischemic brain tissue, such as ionic imbalance, mitochondrial dysfunction, blood-brain barrier (BBB) dysfunction, neuroinflammation, and neuronal death. The degree of tissue injury acquired physical disability and mortality depends on the restoration of central blood flow (Sims and Muyderman, 2010) (Kuriakose et al., 2020). Hence, the restoration of blood flow plays an essential role in stroke recovery.

1.2 Restoration of blood-flow

The cerebral vasculature provides oxygen and nutrients to the brain. Although the cause of stroke is vascular, its consequences are parenchymal. Restoration of blood flow by thrombolysis or thrombectomy is the only efficacious option for saving life and preventing long-lasting disabilities. During acute flow obstruction, the core region of the stroke suffers from ischemia; however, some tissue is sustained by collateral flow through pre-existing anastomoses. Therefore, collateral flow recruitment plays a critical role in the non-interventional treatment of stroke (Liu et al., 2014). Clinical evidence suggests that the collateral status is an independent predictor of the outcome and response to

recanalization therapies in patients experiencing ischemic stroke (Menon et al., 2011, Miteff et al., 2009)

Arteriogenesis refers to the remodeling (specifically, an increase in the diameter) of pre-existing collateral arteries attributed to mechanical forces (elevated pressure) secondary to the supply artery's occlusion. Angiogenesis is a physiological process due to the insufficient local supply of oxygen and hypoxic tissues that upregulate the expression of proangiogenic growth factors (Scholz et al., 2001). New vessels, such as sprouts or offshoots of the pre-existing microvasculature, are induced within 4 to 7 days after cerebral ischemia at the border of the ischemic core and its periphery (Kanazawa et al., 2017). These sprouts are thought to extend until they connect with other sprouts or capillaries and are finally converted into new blood vessels. Both arteriogenesis and angiogenesis increase the collateral flow, providing blood and nutrients to the affected area, which improves the recovery from stroke.

1.3 Animal stroke models

Intraluminal transient middle cerebral artery occlusion (tMCAO) is widely considered a suitable model for mimicking human ischemic stroke. The rat model was developed by Koizumi in 1986 (Koizumi, 1986). It has been widely used to clarify mechanisms of brain injury and recovery from ischemic stroke, as well as to explore potential therapies. The technique was modified further to take advantage of transgenic and knockout strains (Fujii et al., 1997). Further improvements in the model include alterations in the size, shape, and entry points of the monofilament used for vascular occlusion. Although the entry points may differ between techniques, the monofilament is advanced to the offspring of the middle cerebral artery (MCA) from the circle of Willis, thereby blocking the blood flow to the MCA. Stroke severity is regulated by varying the reperfusion intervals following monofilament-mediated MCA blockage. The reperfusion interval used in the studies shown below varies from 20 minutes to 40 minutes **(Fig. 1).**

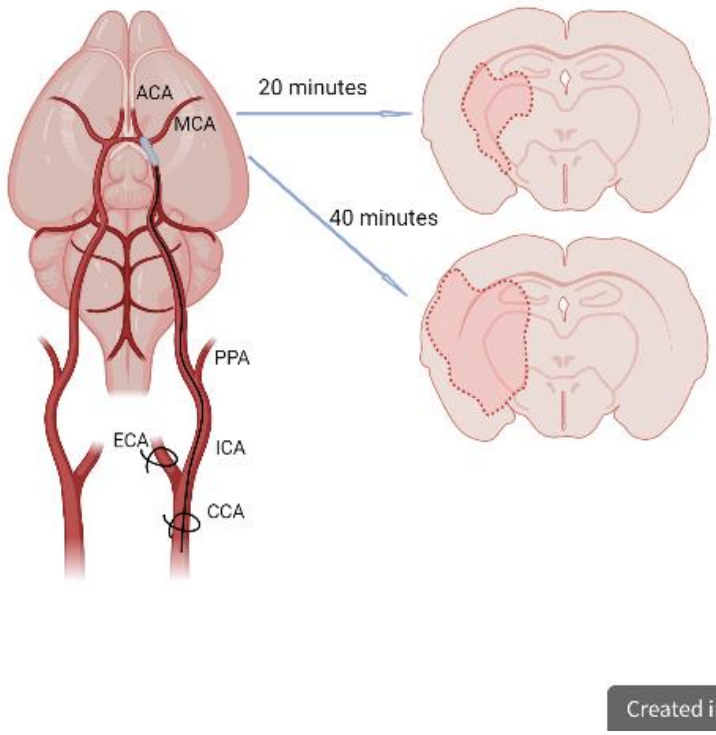

Figure 1. Schematic illustration of the intraluminal tMCAO model.
Depiction of typical lesion size following 20 and 40 minutes of occlusion in the proximal MCAO model. MCAO: middle cerebral artery occlusion; CCA: common carotid artery; ECA: external carotid artery; ICA: internal carotid artery; PPA: pterygopalatine artery; ACA: anterior cerebral artery; MCA: middle cerebral artery.

1.4 Light-sheet microscopy and imaging

Imaging enables quantification of the number and length of blood vessels, evaluation of the blood flow, and measurement of the sizes of the anatomical structures (McDonald et al., 2003). Triphenyl tetrazolium chloride (TTC) and cresyl violet staining are routinely used to determine the area and volume of a cerebral infarct, and microscopic techniques, such as fluorescence, confocal, multiphoton, and electron microscopic imaging, are used to elucidate the structures of blood vessels and other tissues. These methods mainly rely on histological tissue sections, which are enhanced with immunohistochemical staining of endothelial cell markers. The appearance of blood vessels and other tissues in the histological sections is greatly influenced by the section thickness. Even thicker sections contain only parts of the vascular network and other tissues, and the three-dimensional

(3D) architecture and functionality of vessels cannot be adequately considered (Kiessling et al., 2010). Confocal fluorescence microscopy can provide 3D images, but only for stacks of less than 500 nm in thickness. Light-sheet fluorescence microscopy (LSFM) enables the user to perform more practical 3D-imaging.

Siedentopf and Zsigmondy first used light-sheet microscopy for the visualization of small colloidal particles (Siedentopf et al., 1902). For illumination of a well-defined volume, they created a sheet of light by using lenses, aperture stops, and microscope objectives (Keller et al., 2012). However, lasers were not available at that time. In recent years, LSFM was adapted for imaging of biological specimens, e.g., the adult mouse brain (Pampaloni et al., 2015). This version of LSFM consists of detection apparatus, such as a modern charge-coupled device or complementary metal-oxide-semiconductor camera, as well as an illuminator, specimen chamber, and computer-controlled motorized micropositioners for specimen movement. These components enable the imaging of thicker tissues with an excellent dynamic range, high quality, and high sensitivity (Santi, 2011; Pampaloni et al., 2015). LSFM incorporates excitation and detection paths. The excitation path is perpendicular to the detection path, and a laser light sheet is directed such that it illuminates a thin slice of the sample. The light sheet is moved through the specimen, and images are recorded in different planes along the optical axis of the detection lens; the images are 3D-reconstructed with computer software (Stelzer, 2015). LSFM is a very efficient method for the 3D-reconstruction of tissue structures without serial sectioning, although the quality depends on the transparency of the sample (Conchello et al. 2005). Many tissue clearing methods have been developed to achieve tissue transparency. For vessel staining and LSFM, these methods are aqueous- or solvent-based and are vastly beneficial to the study of mouse and human vasculature (Qi et al., 2019).

1.5 Vessel staining

The microvasculature plays a crucial role in maintaining tissue homeostasis, for instance, by modulating oxygen transport and nutrient delivery. Structural changes to the microvasculature are related to numerous diseases, e.g., microangiopathy and stroke

(Pantoni). In addition, the microvasculature is recognized as one of the most promising routes of drug delivery for direct targeting of microvascular endothelial cells. However, first of all, the substance must pass through the BBB by passive and active transport. The main passive pathway is through free diffusion for lipid-soluble molecules and low molecules with masses below 400-600 Da (Pardridge et al., 1999). The active transport system of cells is mostly via carrier-mediated transport, receptor-mediated transport, or absorptive-mediated transport (Pardridge et al., 2001). Drugs mainly traverse the BBB via active transport to reach the endothelial cells. Thus, research focused on microvascular structures is vital. The classical method of studying the microvasculature involves labeling of cell types, distinct marking of unique basement-membrane constituents, or intravascular injection of a dye, followed by high-resolution imaging. An example is lectin staining, labeling the blood vessels with superfused IB4; however, this method also labels pericytes and macrophages. With CD31, the endothelial cells are labeled, as well as platelets and T cells, and, with vWf, the endothelial cells are labeled along with megakaryocytes. Thus, all classical immunological methods of studying microvasculature have downsides, as one cannot be certain of the cell type that is immunostained (Allinson et al., 2012; (Corliss et al., 2019). In this context, we utilized a straightforward method for the labeling and imaging of vessels with LSFM, combining 3D solvent-based clearing with the systemic injection of a gelatin hydrogel containing fluorescein isothiocyanate (FITC)-conjugated albumin (Tsai et al., 2009, Ertürk et al., 2012).

1.6 Optical tissue clearing

Scientists have long realized that thicker sections are more difficult to image because a higher tissue volume causes the light scatter to become obscured. Incident light that passes through a material is refracted by its interaction with many molecules, extracellular fluid, and electrons. The refractive index changes at the interface between two materials, which is why a heterogeneous substance has a milky appearance. The goal of tissue clearing is not to prevent scattering (which is only possible in a vacuum) but to assure a highly uniform density within the tissue, allowing all wavelengths of light to pass through the tissue (Richardson and Lichtman, 2015). Numerous tissue clearing methods have been

developed to address light scattering in tissues and improve high-resolution image acquisition. Two of the most common clearing methods include solvent-based clearing and emerging aqueous-based techniques. Aqueous-based clearing is an approach in which the sample is immersed in an aqueous solution with a refractive index between 1.44 - 1.52, matching the average RI of most tissues. The advantage of this method is that it preserves lipids and is therefore compatible with lipid staining. However, the disadvantage is that it is not very effective for large samples, for example, the entire mouse brain. Solvent-based clearing materials are composed of tissue dehydrating solutions, such as tetrahydrofuran (THF) and refractive index-matching solutions, e.g., ethyl cinnamate (ECi) or dibenzyl ether (DBE) (Merz et al., 2019; Lugo-Hernandez et al., 2017). THF removes water and solvates some of the lipids, which results in relatively homogenous tissue, and ECi or DBE solvates additional lipids to match the higher refractive index of the defatted and dehydrated tissue (Richardson and Lichtman, 2015). However, both approaches have certain drawbacks. Solvent-based clearing yields sufficient transparency of the mouse brain but can cause rapid quenching of endogenous fluorescence (Jing et al., 2018, Ertürk et al., 2012). In contrast, aqueous-based clearing requires long incubation steps and often yields insufficient transparency (Susaki et al., 2014, Lai et al., 2018).

1.7 Therapeutic strategies for the treatment of stroke and post-stroke inflammation

Ischemic stroke is the leading cause of long-term disability, imposing an economic burden on society (Benjamin et al., 2019, Johnson et al., 2016). Therapeutic options are limited to thrombolysis and thrombectomy. Currently, ischemic stroke is treated with thrombolytic agents, such as recombinant tissue plasminogen activator (rt-PA), or with surgical thrombectomy to mechanically remove the clot (thrombus) (Prabhakaran et al., 2015). Existing evidence suggests that the benefits of rt-PA therapy outweigh the risks for patients who present within 4.5 hours of stroke onset. The first randomized clinical trial evaluated 624 patients with ischemic stroke who presented within 3 hours of symptom onset. Patients receiving intravenous rt-PA had a 16% absolute increase in favorable outcomes over 3 months compared to placebo (National Institute of Neurological

Disorders, Stroke rt-PA Stroke Study Group 1995). Other thrombolysis has been administered for acute ischemic stroke, such as intra-arterial recombinant prourokinase. Subsequent studies confirmed this action, and the therapeutic window could be extended to 4.5 hours, which is largely still valid today (Hacke et al., 2008).In the other hand, the FDA has approved several mechanical thrombectomy devices based on technical efficacy and safety that were shown in randomized controlled clinical trials (Nogueira et al., 2012, Saver et al., 2012, Smith et al., 2008, Smith et al., 2005). However, the treatment requires advanced equipment, experienced surgeons, and generates high costs, making it difficult to implement it in low income countries. Many neuroprotective drugs have been studied in the delayed phase of stroke, yet none of those that proceeded to clinical trials have been efficacious in humans. Thus, scientists have been continuously exploring treatments, with inflammation currently being considered an important target for the development of stroke therapies.

Post-ischemic inflammation is a crucial process in the progression of brain ischemia-reperfusion injury, which can seriously affect stroke-related outcomes(Stoll and Nieswandt, 2019). The occlusion of blood vessels, derived from thrombosis and embolisms, induces hypoxia and glucose deprivation in brain tissue. The resulting ischemia causes oxidative stress by releasing, reactive oxygen species (ROS) and reactive nitrogen species (RNS). Together with proteinases, they alter the permeability and enhance the breakdown of the BBB (Yoshimura et al., 2012, Rodrigo et al., 2013). Brain cells, including astrocytes, oligodendrocytes, and microglia cells, produce many chemokines, which attract monocytes, macrophages, neutrophils, and other immune cells to infiltrate the ischemic tissue when the BBB is broken. T lymphocytes specifically act as injury mediators after a stroke (Schroeter et al., 1994). The concentration of T lymphocytes close to the affected vessels peaks around day 3 after ischemia, consisting of $CD4^+$ helper T lymphocytes, $CD8^+$ cytotoxic T lymphocytes, and γδ T lymphocytes. These cells produce inflammatory cytokines, such as IL-1ß, TNF-α, IL-23, INF-γ, IL-4, and IL-12, which enlarge the infarct area and increase the chance of brain injury. However, IL-4 and IL-10 may attenuate ischemic damage and promote tissue repair based on a study by Xiong, et al. (Xiong, et al. 2011). INF-γ is considered neurotoxic as it directly induces neuronal cell apoptosis in vitro (Lambertsen et al., 2004). Other cytokines derived from T lymphocytes are also thought to act as neurotoxic effectors, as T lymphocyte-deficient

mice had a statistically significant reduction in infarct volume compared to wild-type mice; the same was not true of B lymphocyte-deficient mice (Yilmaz et al., 2006). Moreover, modifying immune response enhances post ischemic tissue survival and neurological outcomes (Lambertsen et al., 2019, Green et al., 2006).

1.8 FTY720

Fingolimod (FTY720) is a small molecule immunomodulator, which is used for treatment of multiple sclerosis. It is a structural analog of sphingosine and is phosphorylated by sphingosine kinases in the cell (Paugh et al., 2003). Unlike other immunosuppressive agents, which inhibit T cell activation and proliferation, phospho-FTY720 induces the internalization of sphingosine-1-phosphate (S1P) receptors, which sequesters lymphocytes from the circulation to secondary lymph-tissue compartments and concomitantly impedes the recirculation of effector T lymphocytes to the inflamed tissue (Pinschewer et al., 2000; Chiba et al., 1998). FTY720 treatment reduces ischemic brain injury by preventing the egress of lymphocytes from the lymphoid organs, thereby reducing the infiltration of T lymphocytes in the post-ischemic brain and attenuating adaptive immune responses (Kraft et al., 2013) **(Fig. 2).**

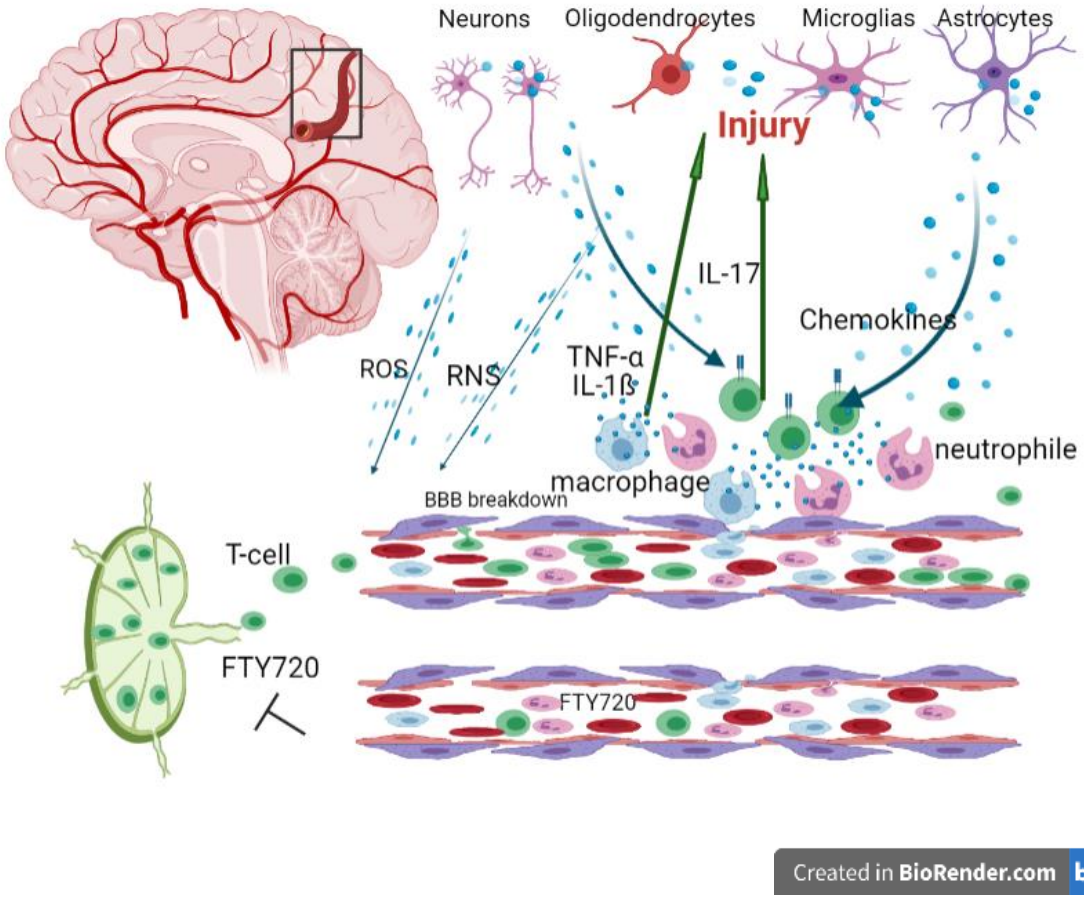

Figure 2. The recruitment of immune cells to the injury site, as modulated by FTY720 after ischemic stroke.

Post-ischemic ROS, RNS, and chemokines released from dying brain cells regulate the permeability of the BBB and break the tight junction. Thereafter, immune cells infiltrate into the ischemic region via the BBB and release multiple inflammatory mediators. These include cytokines derived from T lymphocytes, and act as neurotoxic effectors, injuring brain cells and increasing infarct volume. However, FTY720 can trap T lymphocytes in the lymph nodes, resulting in a decrease of infarct volume. BBB: blood-brain barrier; FTY720: fingolimod; RNS: reactive nitrogen species; ROS: reactive oxygen species.

AIM OF THE STUDY

Microvascular remodeling, including angiogenesis, has profound implications for the brain recovery after an ischemic stroke (Hermann and Chopp, 2012). Although FTY720 is primarily used in the treatment of multiple sclerosis, it has recently been reported to have a protective effect after stroke. In this study, we aimed to (1) 3-dimensionally reconstruct and quantify microvessels in ischemic mouse brains in a time-resolved manner; (2) observe the differences in microvessel remodeling following mild vs. severe stroke; and (3) study the effect of FTY720 treatment on the vasculature after ischemic stroke induced by intraluminal MCAO in mice.

MATERIALS AND METHODS

1.9 Animals

All experiments were performed with local government approval (Bezirksregierung Düsseldorf) and complied with the EU guidelines for the Care and Use of Laboratory Animals and the ARRIVE guidelines. Male C57BL/6J mice (25-30 g body weight, 10-12 weeks old) were kept in a consistent light-dark cycle (12-h shifts) in groups of five animals per cage, with free access to food and water. Mice with respiratory abnormalities or severe motor disabilities after tMCAO resulting in weight loss > 20% were excluded from the study. The animal experiments was completely blinded at all stages of the study. Another researcher prepared vehicles and medicines for treatment. These treatments were allocated dummy names that were only unblinded after the termination of the study.

1.10 Induction of focal cerebral ischemia

Focal cerebral ischemia was induced using an intraluminal filament technique with minor modifications. Anesthesia was induced in the mice with 5% isoflurane (in 30% O_2 and 70% N_2O) and maintained with 1.0-1.5% isoflurane. The rectal temperature was maintained between 36.5 and 37.0°C by using a feedback-controlled heating system. Buprenorphine (0.1 mg/kg, s.c.; Reckitt Benckiser, Slough, UK) was injected into the mice preoperatively. Laser Doppler flowmetry (Müller et al., 1994) was performed with a flexible probe placed above the core of MCA territory for up to 15 minutes after monofilament removal to confirm successful ischemia and reperfusion. An incision was made on the midline of the neck to expose the left common carotid artery, internal carotid artery (ICA), and external carotid artery (ECA) (Allinson et al., 2012). Subsequently, the CCA and ECA were ligated, and the ICA was temporarily clipped. A silicon-coated monofilament (Doccol Corp., Sharon, MA, USA) was inserted via a small incision in the CCA, to obstruct the MCA. Following occlusion, the LDF signal decreased. Control animals underwent sham surgery consisting of anesthesia and carotid artery exposure alone. After 20 or 40 minutes of occlusion, the filament was removed to induce

reperfusion, resulting in the restoration of the LDF signal. Thereafter, carprofen (4 mg/kg per day, s.c.; Norbrook, Newry, UK) was administered for post-operative pain relief during the first 3 days after surgery. The exclusion criteria were as follows: (1) prolonged surgery (duration > 40 or 60 minutes); (2) insufficient drop of blood flow (< 75%) after occlusion; (3) lack of reperfusion after monofilament withdrawal, and (4) > 20% weight loss and respiratory abnormalities.

Table 1. Surgical materials and equipment used for induction of focal cerebral ischemia

Materials and equipment	**Manufacturer**
Carl Zeiss OPMI surgical microscope	Carl Zeiss, Oberkochen, Germany
Feedback-controlled heating system	Harvard Apparatus, Holliston, MA, USA
Halsey micro needle holder (Manoonkitiwongsa et al. 12500-12)	Fine Science Tools, Heidelberg, Germany
Laser Doppler flowmetry system (Müller et al., 1994)	Perimed Instruments, Rommerskirchen, Germany
Silicon-coated monofilament (Manoonkitiwongsa et al. 702234PK5Re)	Doccol, Sharon, MA, USA
Silk suture 5-0 (Manoonkitiwongsa et al. K890H)	Ethicon, Norderstedt, Germany
Silk suture 7-0 (Manoonkitiwongsa et al. EH7464G)	Ethicon, Norderstedt, Germany
Spring scissors (Manoonkitiwongsa et al. 15024-10)	Fine Science Tools, Heidelberg, Germany
Standard scissors (Manoonkitiwongsa et al. 14568-12)	Fine Science Tools, Heidelberg, Germany
Vannas spring scissors (Manoonkitiwongsa et al. 15000-00)	Fine Science Tools, Heidelberg, Germany
Vascular clip, 9-mm long (Manoonkitiwongsa et al. FD562R)	Fisher Scientific, Schwerte, Germany

1.11 Group allocation

In total, 270 male mice were divided into five sets: set I, sham-operated mice (control, n=10); sets II and III, mice subjected to tMCAO (filament inserted for 20 or 40 minutes, respectively), fed with standard ad libitum diet which were sacrificed 3 hours, 24 hours, 3 days, 7 days, 14 days, 28 days, or 56 days post-ischemia. 5-21 mice were involved in each group at each time point. Sets IV and V were subjected to tMCAO (filament inserted 20 or 40 minutes, respectively), fed ad libitum and treated with daily intraperitoneal injections of vehicle or FTY720 (1 mg/kg) for 7 days or 14 days. 5-15 mice were involved in each group at each time point.

1.12 Hydrogel preparation

A hydrogel was prepared for labeling of the vasculature. In brief, phosphate-buffered saline (PBS) was heated to 90°C and thereafter cooled down to 60°C. Gelatin was added at a concentration of 2% (w/v) and allowed to cool down to 40°C with constant stirring. Thereafter, fluorescein isothiocyanate (FITC)-conjugated albumin was added to the gelatin solution at a concentration of 0.1% (w/v). The gel was filtered by using filter paper (GE Whatman, Dassel, Germany) and continuously stirred at 37°C to avoid excessive evaporation.

1.13 Animal sacrifice and hydrogel perfusion

Animals were deeply anesthetized with isoflurane and subjected to transcardial perfusion of 40 mL of heparinized (50 U/mL of heparin; Ratiopharm, Ulm, Germany) 0.01 M PBS, followed by perfusion of 40 mL of 4% paraformaldehyde (PFA; Merck-Millipore, Darmstadt, Germany) in PBS. Thereafter, in animals used for light-sheet microscopy, 10 mL of the hydrogel was infused. The mice were immediately placed with their heads downward into ice water for 15 minutes. The brains of all mice were carefully removed and incubated in 4% PFA at 4°C overnight.

Table 2. Hydrogels and staining materials for microscopic imaging

Staining	Catalogue number	Company
Gelatin	9000-70-8	Sigma-Aldrich, Deisenhofen, Germany
PBS tablets	524650	Merck-Millipore, Darmstadt, Germany
FITC-conjugated albumin	A9771	Sigma-Aldrich
Filter paper	1213-125	GE Whatman, Dassel, Germany
Heparin	N68542.05-Z01	Ratiopharm, Ulm, Germany
Paraformaldehyde	P6148	Merck-Millipore

1.14 Whole-brain clearing

Samples were prepared as previously reported by Lugo-Hernandez (Lugo-Hernandez et al., 2017) The procedure involved two steps: dehydration and refractive-index matching. Brains were incubated in 20 mL of gradient THF (Sigma-Aldrich; 30%, 60%, 80%, 100%, and 100%) for dehydration at room temperature for 12 hours each after the overnight fixation in 4% PFA solution. The samples were gently moved throughout this process at 60 rpm by using a horizontal shaker. Finally, the samples were transferred into ECi solvent (Sigma-Aldrich) for 12 hours with continuous agitation and stored in the solution until image acquisition. The entire procedure was performed in dark brown glass bottles to protect samples from exposure to direct light. A length correction factor of 1.318 was used to correct the final analysis because of the dehydration-induced reduction in brain size.

1.15 LSFM and image processing

Samples were imaged by using a commercial light-sheet microscope (UltraMicroscope II, Miltenyi Biotec, Bergisch Gladbach, Germany), consisting of ImSpector software, a 2560 × 2160 px chip with a 6.5-µm pixel size, and a 2× 0.5 objective lens fitted with a dipping cap, fitted into an MVX10 zoom microscope body (Olympus Corp., Tokyo, Japan;

magnification range of 0.63× to 6.3×). The mouse brains were subjected to serial optical imaging. First, brains were mounted in a sample holder in the ventral-dorsal direction, and placed in a chamber filled with ECi. The FITC-conjugated albumin-labeled vessels were excited at 488 nm and captured at 525/50 nm band-pass emission. Autofluorescence was excited with a 561 nm laser and detected by using a 595/40 nm band-pass emission filter.

Whole-brain scanning was used to analyze the infarct and striatum volumes, and an individual overview was used as a reference in the selection of regions of interest (ROIs). Both were acquired at a total magnification of 1.6×. In general, whole-brain measurements required approximately 500-600 image stacks at 10 µm step-size intervals. Each brain hemisphere was captured at 6.4× magnification with a 2 µm step size in the axial direction by using dynamic focus and the highest numerical aperture of the light-sheet illumination for optimal axial resolution. For consistent imaging between samples, the first image was taken at bregma −6.24 mm, the same as for the overview image, and the last at bregma −5.24 mm, resulting in the acquisition of 501 images each for the ischemic (ipsilateral) and non-ischemic (contralateral) hemispheres. Another two image stacks for each hemisphere were acquired, one from bregma −2.74 mm to bregma −2.04 mm (351 images), and the other from bregma −3.04 mm to bregma −2.44 mm (301 images), all in the ventrodorsal direction with a 2 µm step size.

Table 3. Material for sample dehydration and cleaning

Name	Catalogue number	Company
Tetrahydrofuran	102116439	Sigma-Aldrich
Ethyl cinnamate	102051821	Sigma-Aldrich
DPBS (Dulbecco's phosphate buffered saline)	21300-058	Gibco, Life Technologies Corporation
Isoflurane	440532079	Piramal Critical Care Deutschland GmbH, Hallbergmoos, Germany

1.16 Vascular quantification of light-sheet images

For detailed vascular quantification in stroke brains, two software programs (ImageJ and Imaris version 9.3.1 [Oxford Instruments plc, Abingdon, UK]) and Python programming were used. First, the open-source software, ImageJ, was used to pre-process the image data by applying Gaussian smoothing (sigma = 2) followed by rolling-ball background subtraction (radius = 20). Subsequently, a total of 4 ROIs were selected for each brain hemisphere in ImageJ.

The four ROIs (RA, RB, RC, and C2) were defined from an overview image acquired at bregma −6.24 mm by drawing a guideline, orthogonal to the brain midline and crossing through the round opening at which both lateral ventricles are connected with the third ventricle. The point at which the guideline passed through the border between the striatum and adjacent cortex marked the position of the ROIs. RA, RB, and RC measured 508 × 508 × 1000 µm at the infarct core and covered the dorsolateral pole of the striatum. RC was the farthest from the infarct core on the ventral side of the striatum. C2 was an ROI of 300 × 300 × 600 µm, located in the cortex adjacent to RB. All four ROIs were first selected in the ischemic hemisphere; thereafter, ROIs were selected in the corresponding positions in the non-ischemic hemisphere.

Second, a Python script, derived from the Vascular Modeling Toolkit (vmtkimagevesselsenhancement; VMTK: www.vmtk.org), based on a multi-scale, Hessian-based Frangi vesselness filter, was used to enhance the vessel contrast for the ROIs. Finally, the image, as processed with ImageJ and the Frangi filter, was imported into Imaris for analysis of dendrite length and branching points.

The Frangi-filtered images were imported into Imaris as the first working channel to analyze the dendritic length and branching point above the vessel's diameter of 5 μm by imaris. The filament-tracing algorithm was used to calculate an automated segment-vessel threshold. The following parameters were selected: connective baseline segmentation, 700-900; approximate diameter, 3 μm; and the minimal ratio of branch length to trunk radius, 3. Frangi vesselness filtering may cause branching point discontinuity, particularly for branches that originate orthogonally to the main branch. Moreover, the intensities of smaller vessels may be disproportionately amplified compared to those of larger vessels. These errors can affect the vessel-diameter analysis during filament tracing in Imaris. Therefore, after creating the initial filament model with Frangi-filtering, the original images from the Image as the final working channel were utilized to re-align against the channel to trace the dendritic length. Consequently, the overall statistics, including blood vessel diameter, total vascular length, and total vascular volume, were exported for data analysis **(Fig. 3)**.

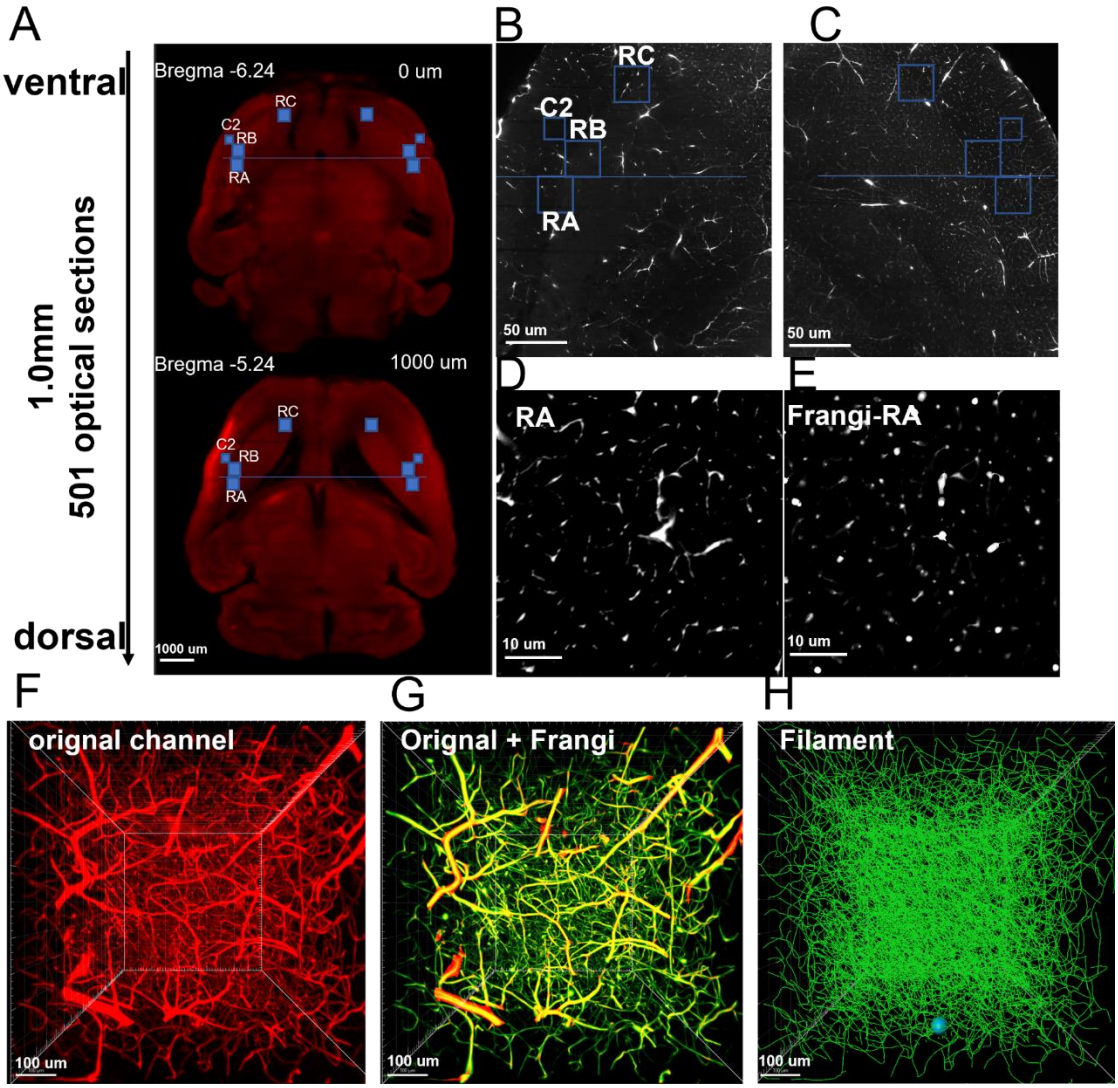

Figure 3. Analysis of ventral and dorsal brain regions.

A. ROI was defined with a line drawn through the circular opening of the two lateral ventricles connected to the third ventricle. The scale bar represents 100 µm. **B-C.** RA and RB were measured at the infarct core as 508 × 508 × 1000 µm, and RC was the farthest location of the striatum ventral to the infarct core. C2 was a 300 × 300 × 600 µm ROI located in the cortex near RB. The scale bar represents 50 µm. **D-E.** Subsequently, the images were processed using ImageJ utilizing Frangi filters function. The scale bar represents 10 µm. **F-G-H.** The original ones merged with Frangi-filtered images were imported into Imaris as a working channel. Dendrite length and branching points were analyzed with a semi-manual filament tracking tool. The scale bar represents 100 µm.

Table 4. Equipment and analysis software for imaging

Name	Company
Light-sheet fluorescence microscopy (LSFM): UltraMicroscope II	Miltenyi Biotec
Leica Application Suite X	Leica Microsystems GmbH, Wetzlar, Germany
ImageJ	Open-source
Imaris software	Oxford Instruments plc

1.17 Brain infarct and striatum volumetric analysis

Brain infarct and striatum volumes were measured by using the volume and surface tools in Imaris. Whole-brain images were rendered by default with maximum intensity projection, based on an autofluorescence signal at a wavelength of 595 nm that sharply distinguished brain infarct tissue from the surrounding tissue. The normal shading module was utilized by adjusting the minimum and maximum voxels in order to display the correct infarct area. Subsequent image processing was performed in the surface module. Briefly, the surface was created only for each ROI. Thereafter, the standard rectangle was adjusted for approximate selection of the infarct region, and the threshold of absolute intensity was adjusted accordingly. A filter was added to clean unwanted spots. Finally, all statistics were exported for analysis.

The striatum volume of interest was also measured by using the surface module. The contour of the striatum was drawn on the corresponding single plane in the coronal direction, starting at the position where the two corpora callosa are connected and extending 1000 μm caudally. The contours were drawn for sections at 200 μm intervals, for a total of six sections. Finally, the surface was created, and all statistics were exported for analysis **(Fig. 4)**.

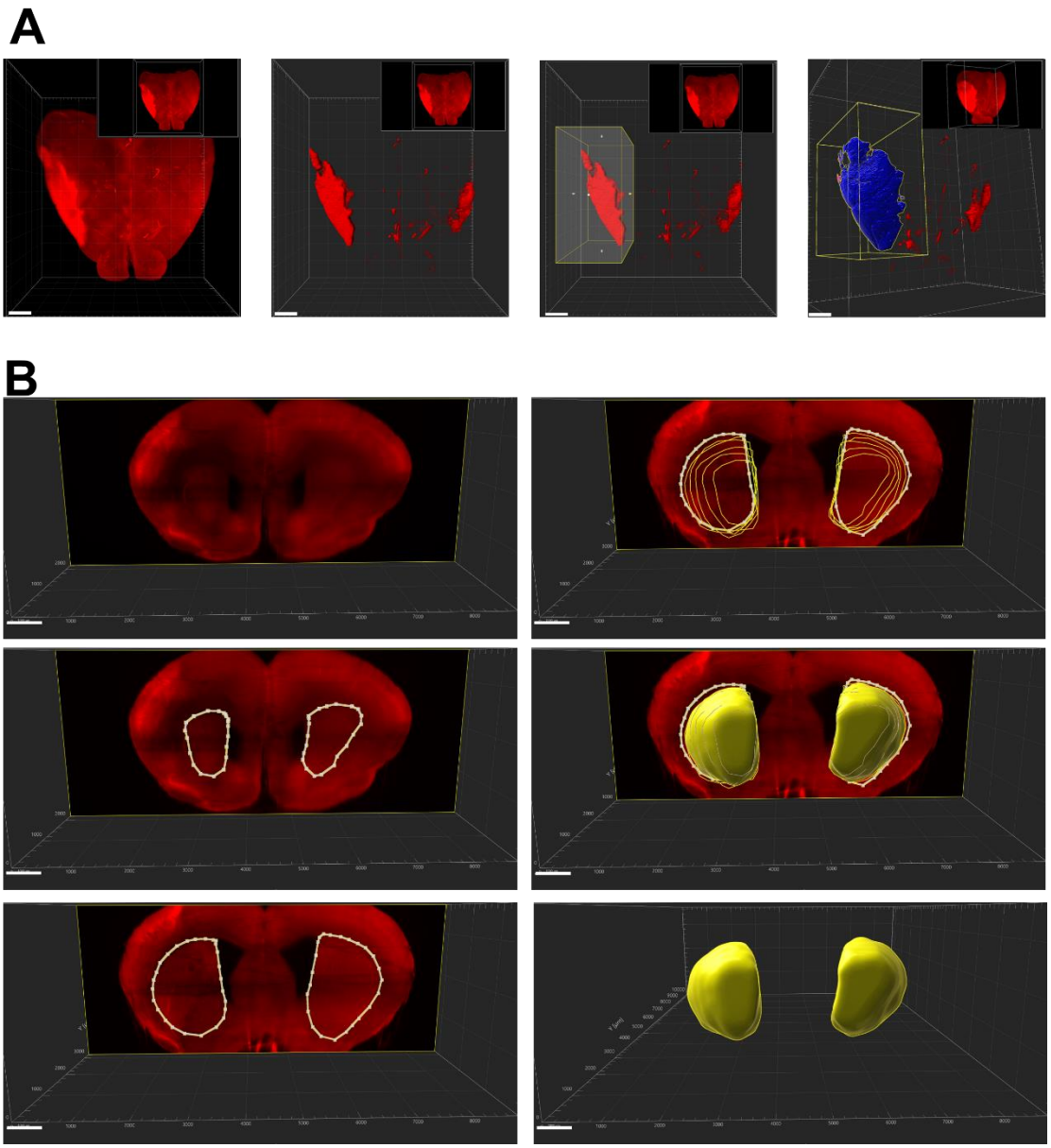

Figure 4. Analysis of brain infarct and striatum volume.

A. Whole-brain images were loaded in Imaris, and brain infarct tissue was clearly distinguished from surrounding tissues based on autofluorescence signals, and subsequently, infarct volumes were created and analyzed. The scale bar represents 1000 µm. **B.** At first, the striatum was found in the coronal position, followed by contour lines drawn at 200 µm intervals up to 1000 µm, for a total of 6 contour lines outlining the interesting striatal volumes, after which these contours were merged using the same surface module, and finally, the volumes were measured, and the data were exported. The scale bar represents 1000 µm.

1.18 Statistical analysis

All data values are presented as means ± standard deviation or box blots with median/mean±interquartile range with minimum and maximum data as whiskers. Data were analyzed by using a two-way analysis of variance followed by the least significant difference post hoc testing to determine significant differences between ischemic and non-ischemic brain areas. P values of $\leqslant 0.05$ were considered statistically significant. Statistical analysis was performed by using GraphPad Prism 7.0.0 for Windows (GraphPad Software, San Diego, CA, USA).

RESULTS

1.19 Analysis of infarct volume and shrinkage of striatal volume after stroke

This study aimed to gain an in-depth understanding of the 3D structure of cerebral blood vessels after mild or more severe ischemia. To this end, mice were subjected to 20- or 40-minute MCAO, and brain blood vessels were subsequently labeled using a fluorescent marker. Light-sheet microscopy allowed spatial imaging of the whole brain or detailed imaging of blood vessels in specific stroke-affected regions in the ischemic hemisphere or the corresponding regions in the non-ischemic hemisphere. Furthermore, the autofluorescence of brain tissue was used to quantify infarct or striatal volume utilizing rendering of whole brain scans in Imaris software. The number of mice in each group at each time point was between 4 and 21. **Figures 5−8** illustrate the autofluorescence signal in whole-brain scans of mice perfused with FITC-conjugated albumin-containing hydrogel after 20 minutes and 40 minutes of tMCAO. The volume or surface area of the infarct region was represented by high-intensity fluorescence **(Fig. 5A, 7A)**. The autofluorescence signal revealed that mice subjected to 20 minutes of ischemia had smaller infarcts than those subjected to 40 minutes of ischemia. After 56 days, the infarct volume was smaller than that at 7 days ($p=0.0208$; **Fig. 5B**), whereas the reduction of the surface area after 56 days did not reach statistical significance ($p=0.0872$; **Fig. 5C**). The difference in the degree of ipsilateral striatal atrophy between mice subjected to mild and severe stroke is demonstrated in Figures **6A** and **8A**. The striatal volume of mice subjected to 20 minutes of ischemia shrank compared to those of naive mice after 14 ($p=0.04$), 28 ($p=0.02$), and 56 ($p=0.0005$) days (**Fig. 6B**).

The infarct volumes of mice subjected to 40 minutes of ischemia showed a continuous decrease starting from day 7 to day 14 ($p<0.0001$), 28 ($p<0.0001$), and 56 ($p<0.0001$; **Fig. 7B**) post-stroke, whereas no infarct could be detected using autofluorescence on day 3 post-ischemia (data not shown). The striatal volume of mice subjected to 40 minutes of ischemia showed a significant increase after day 3, however this volume decreased after

day 14 (p=0.0004), shrinking even further after day 28 (p=0.0013), and day 56 (p<0.0001) **(Fig. 8B)** compared to that of naïve mice.

Fig. 9 illustrates the shrinkage of striatal volume over time, comparing mice with mild stroke and those with severe stroke. The striatal volume was expected to shrink over time after the stroke, with severe stroke leading to greater shrinkage. This hypothesis was able to be confirmed by this study. The increase of striatal volume after 3 days was presumably caused by tissue swelling after injury. From 14 days post-ischemia onward, the striatal volume decreased significantly compared to that of naïve mice. Furthermore, significantly more shrinkage of striatal tissue could be observed in mice with severe stroke when compared to those with mild stroke at 14 and 56 days.

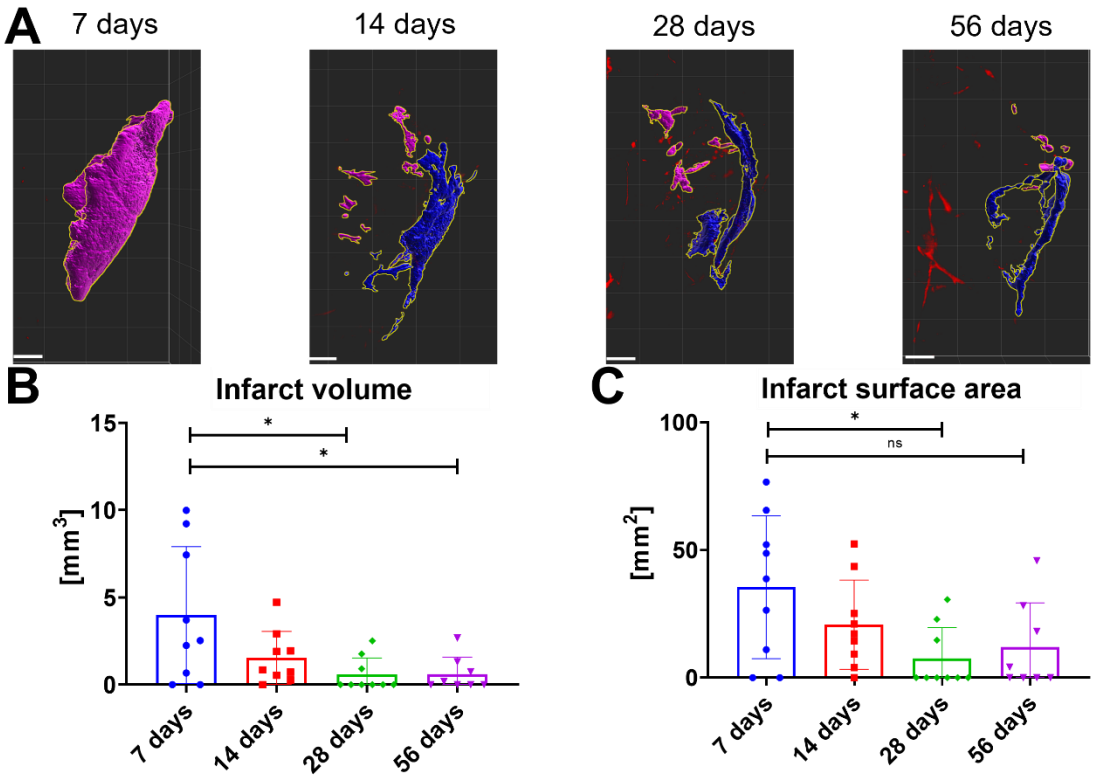

Figure 5. Infarct volumes and surface areas were calculated at 7, 14, 28, and 56 days after mild stroke

A. Representative images of brain infarcts in brains at 7, 14, 28, and 56 days after 20 minutes of ischemia in mice. Tissue autofluorescence was measured in whole brain scans using light-sheet fluorescence microscopy, and the infarcts were analyzed using Imaris volume and surface tools. The scale bars represent 1000 µm. **B-C**. The graphs for infarct volume and infarct area show that both measurements decreased clearly at 28 and 56 days (in **B** only) compared with 7 days post-ischemia.*p<0.05 (n=8-9 animals per group). ns, not statistically significant.

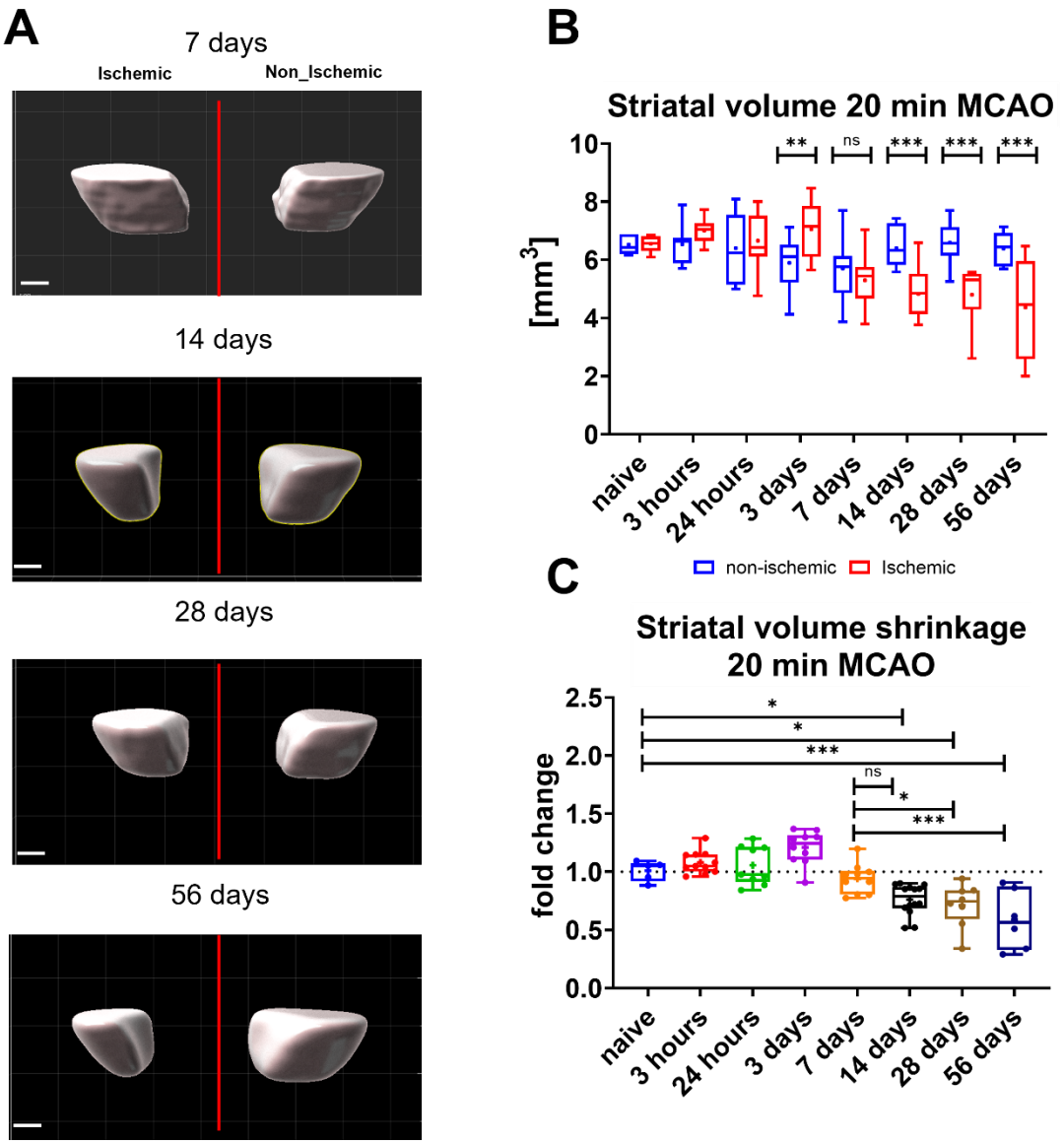

Figure 6. Striatal volumes after mild stroke

A. Representative three-dimensional (3D) striatal images visualized using the surface module in Imaris (left: ischemic, right: non-ischemic). Autofluorescence signals were used in the coronal view to differentiate brain regions. Images at 3 and 24 hours post-stroke are not presented, as the differences were not statistically significant. The scale bars represent 500 µm. **B**. Bar diagrams show the volume of the non-ischemic striatum (blue) and ischemic striatum (red) in mice subjected to 20 minutes of middle cerebral artery occlusion (MCAO), indicating a reduction of striatal volume after 14 days post-ischemia. **C**. Shrinkage of striatal volume as calculated by the ratio between non-ischemic/ischemic volume shows significant tissue shrinkage at 14 days post-ischemia. *p<0.05, **p<0.01, ***p<0.001 (n=8-9 animals). ns, not statistically significant.

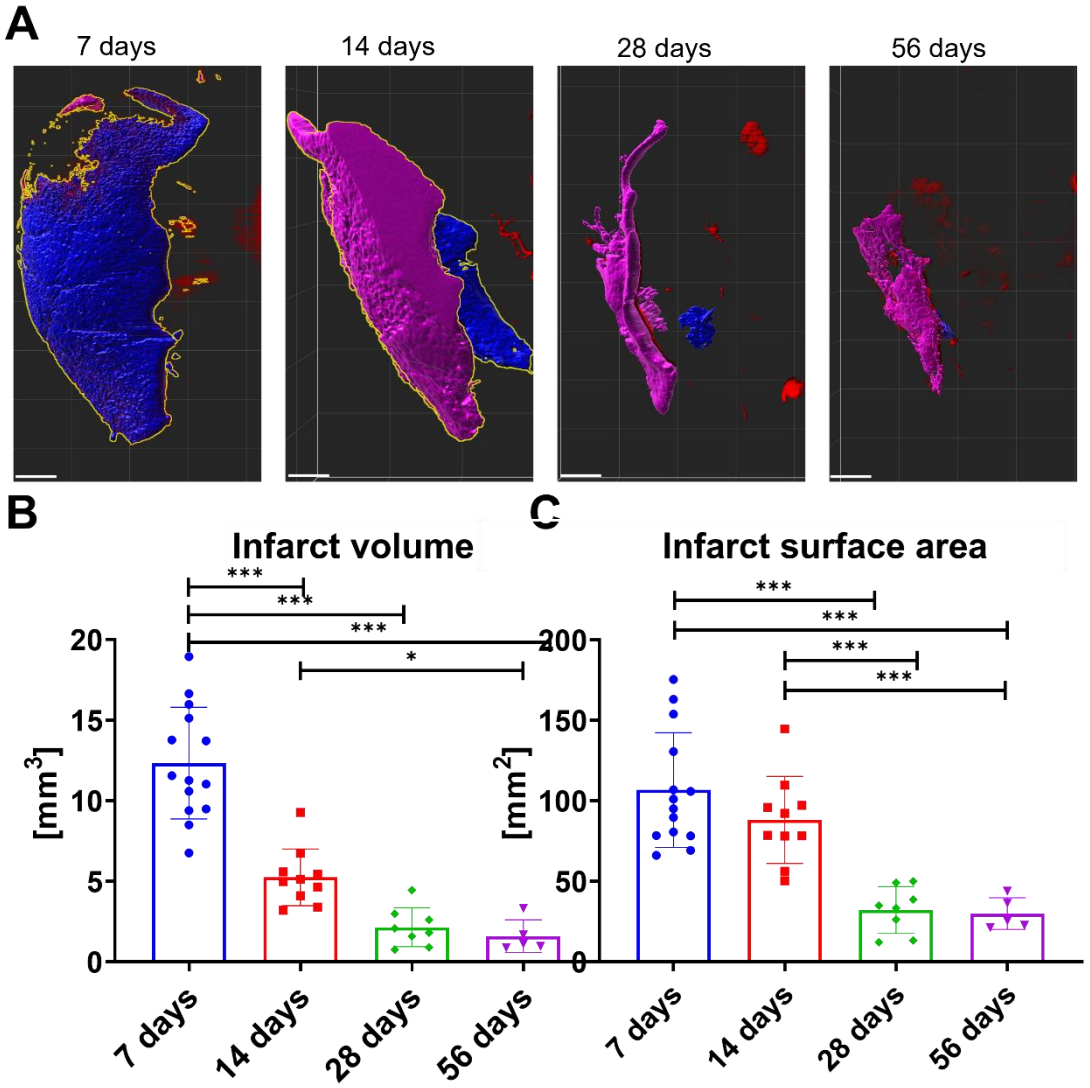

Figure 7. Infarct volumes and surface areas were calculated at 7, 14, 28, and 56 days after severe stroke

A. Representative LSFM images of infarcts in brains obtained 7, 14, 28, or 56 days after 40 minutes of ischemia. Tissue autofluorescence was measured to analyze the infarcts using the Imaris volume and surface modules. The scale bars represent 1000 µm. **B.** Compared with day 7 after the stroke, the infarct volume decreased sharply over time. **C.** The infarct surface areas were calculated automatically by Imaris using the surface module, indicating the reduction at 14 days post-ischemic stroke. There was a significant decrease in surface area on days 28 and 56 compared to days 7 and 14, respectively. *$p<0.05$, ***$p<0.001$ ($n=5-14$ animals per group).

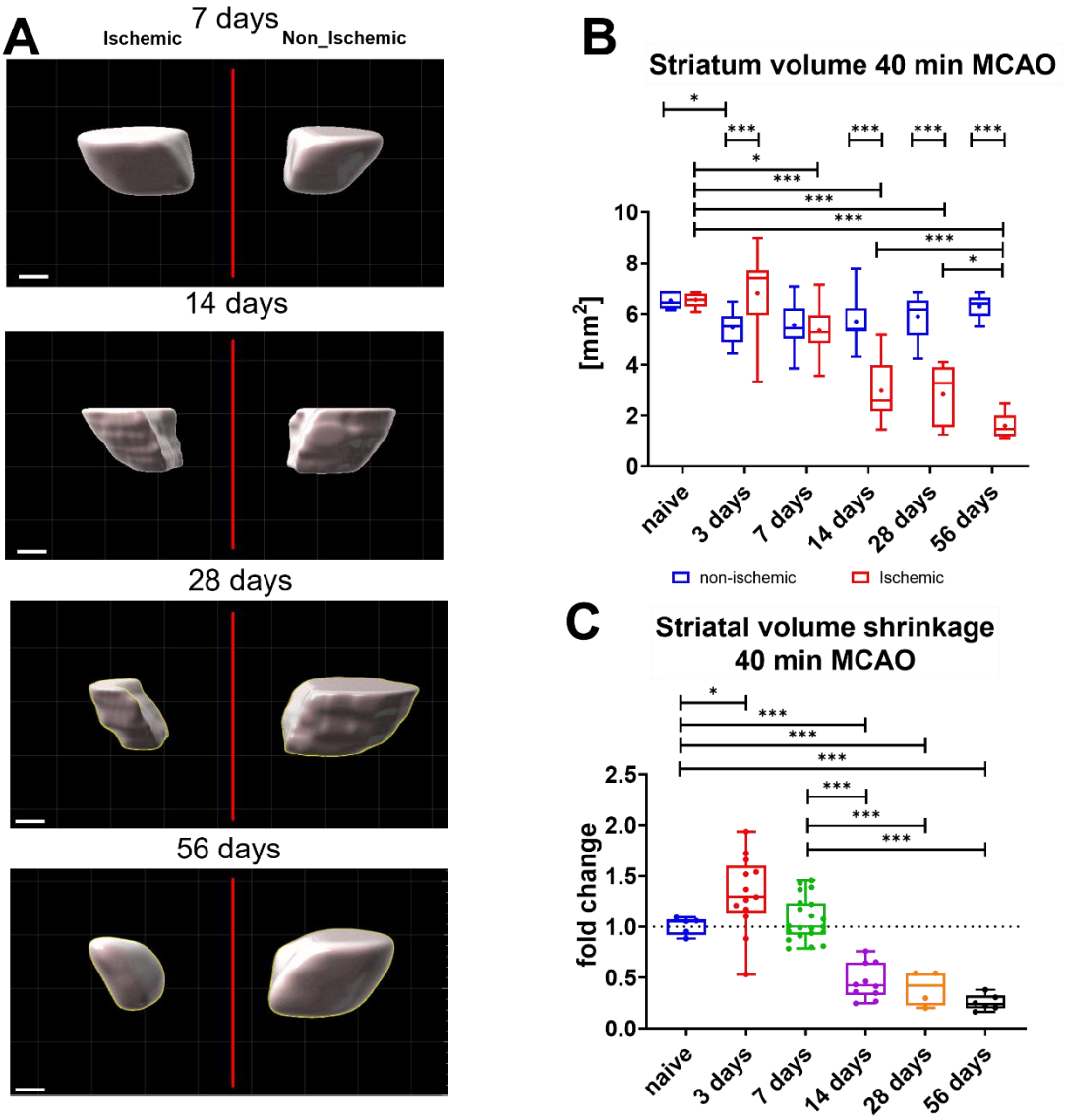

Figure 8. Striatal volumes after severe stroke

A. 3D striatal images visualized using the surface module of Imaris (left: ischemic, right: non-ischemic). Autofluorescence signals of whole brains subjected to 40 minutes of ischemia and perfused at the indicated time points were used to differentiate brain regions. The scale bars represent 500 µm. **B.** Bar graph showing the volume of the non-ischemic striatum (blue) and the ischemic striatum (red), indicating a decrease in striatal volume 14 days post-ischemia. **C.** Reduction in striatal volume calculated from the ratio of non-ischemic/ischemic volume, showing significant tissue atrophy 3 days post-ischemia, but after 7 days, the trend was even more evident. *p<0.05, **p<0.01, ***p<0.001(n=4-21 animals).

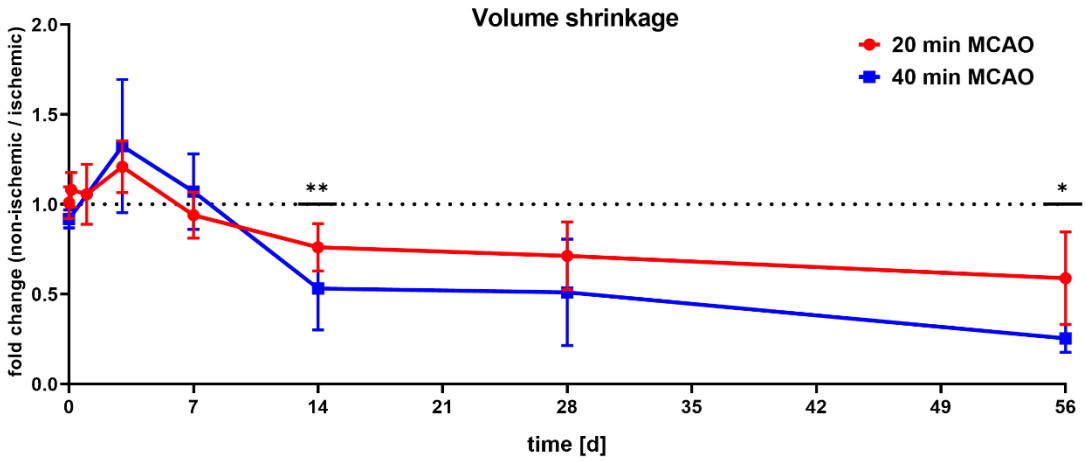

Figure 9. Volume shrinkage of the striatum

The graph illustrates the shrinkage of murine striatal volume from day 0 until day 56 post-stroke for both mild (red) and severe (blue) stroke. The time courses of the lines are very similar; after an increase in striatal volume at day 3, striatal volume is shown to reduce, with a more pronounced reduction in cases of severe stroke. *p<0.05, **p<0.01 (n=5-21 animals per group), middle cerebral artery occlusion (MCAO).

1.20 Vessel length in mice after mild and severe stroke

MCAO blocks the blood vessels, leading to ischemia and hypoxia as well as other nutrient deficiencies in the associated brain region, thus causing loss of the blood vessels. In the present study, we also aimed to investigate, for the very first time, the detailed structure and characteristics of blood vessels after mild and severe ischemia using 3D LSFM. To achieve this, 9−12 weeks old male C57BL/6 mice were subjected to 20 or 40 minutes of MCAO and perfused with fluorescently labeled albumin hydrogel after 3, 7, 14, 28, or 56 days to mark the blood vessels. In addition, naive animals or animals with mild ischemia were also perfused with FITC-albumin hydrogel after 3 and 24 hours, respectively. The brains of the animals were removed and clarified using 3-DISCO technology. Subsequently, the brains were subjected to high-resolution imaging of specific brain regions in the ischemic as well as the corresponding non-ischemic hemisphere using LSFM, and analyzed using the filament tool of Imaris software. For this purpose, regions of interest were identified within the ischemic striatum and in the cortex near the ischemia, with a size of 0.258 mm^3 for the striatum and 0.06 mm^3 for the cortex (**Fig. 3**).

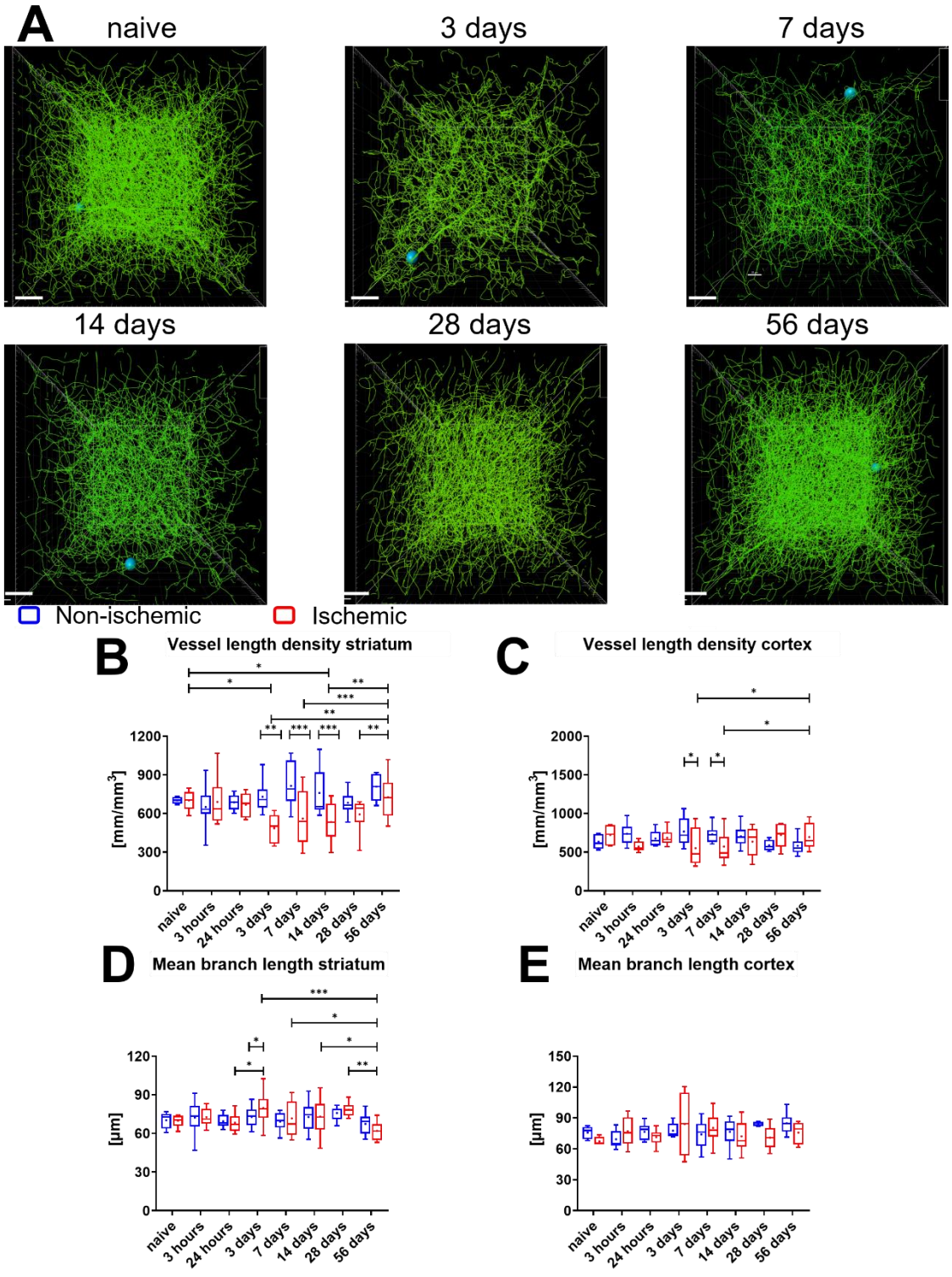

Figure 10 (for figure legend see page 29)

Figure 10. Vessel length density and mean branch length in cerebral microvessels after mild stroke (Figure 10 on page 28).
A. Representative images of microvessels from the filament model in the ischemic striata of male C57BL/6 mice subjected to 20 minutes of middle cerebral artery occlusion (MCAO) and perfused after 3, 7, 14, 28, and 56 days with FITC-conjugated albumin-containing hydrogel for labeling of blood vessels. Microvessels of naïve mice are also shown. Cleared brains were scanned using LSFM, and regions of interest were analyzed using the Imaris filament-tracing tool. Scale bars represent 100 μm**. B and C**. Box-plots show vessel length density (VLD) of cerebral microvessels analyzed in both naïve animals and mice subjected to 20 minutes of MCAO followed by reperfusion for 3 or 24 hours, and at 3, 7, 14, 28, and 56 days in the ischemic (red boxes) or non-ischemic (blue boxes) striatum or the adjacent cortical region. **D and E**. Mean branch length of microvessels was analyzed after the indicated time points in the striatum and cortex after mild ischemia. Data are box plots with medians (lines inside boxes)/means (crosses inside boxes) ± interquartile ranges (IQR; boxes) with minimum/maximum values as whiskers (n=5-15 animals per group). *p<0.05, **p<0.01, ***p<0.001.

Analyses of vessel-length density (VLD) revealed that the first changes occur as early as 3 days after mild ischemia, whereas VLD did not change at earlier time points (3 and 24 hours) in either the striatum **(Fig. 10B)** or the cortex **(Fig. 10C)**. The decreased VLD persists until day 14 post-ischemia in the striatum and day 7 in the cortex. At later time points (28 and 56 days post-ischemia), the VLD in the ischemic hemisphere was equal to that of the non-ischemic hemisphere. In cases of severe stroke, significant changes in VLD were observed in the striatum and cortex 3 days post-ischemia **(Fig. 11B-C)**. VLD significantly decreased in the striatum until day 28 before it reached non-ischemic values at day 56 post-MCAO. However, in the cortex, a significant increase in VLD in the ischemic hemisphere was observed after 56 days compared to the non-ischemic cortex.

VLD declined to a nadir 3 days post-stroke, after which it started to rise, peaking on day 56. In both mice groups, there was no significant difference in VLD between the naïve state and 56 days post-stroke (p=0.7805 and 0.3742, respectively) **(Fig. 10B, 11B)**. The striatal VLD increased at every indicated time point from 3 days post mild stroke, and the increase between days 3 and 56 was statistically significant, both for mice with mild (p=0.0006) and those with severe (p=0.0111) stroke (**Fig. 10B, 11B**).

In addition to VLD, 3D analysis of vessels allowed, for the first time, a detailed analysis of single branches, including the mean branch length (**Fig. 10D, 11D**). Interestingly, we found only slight changes in the mean branch length in cases of both mild and severe

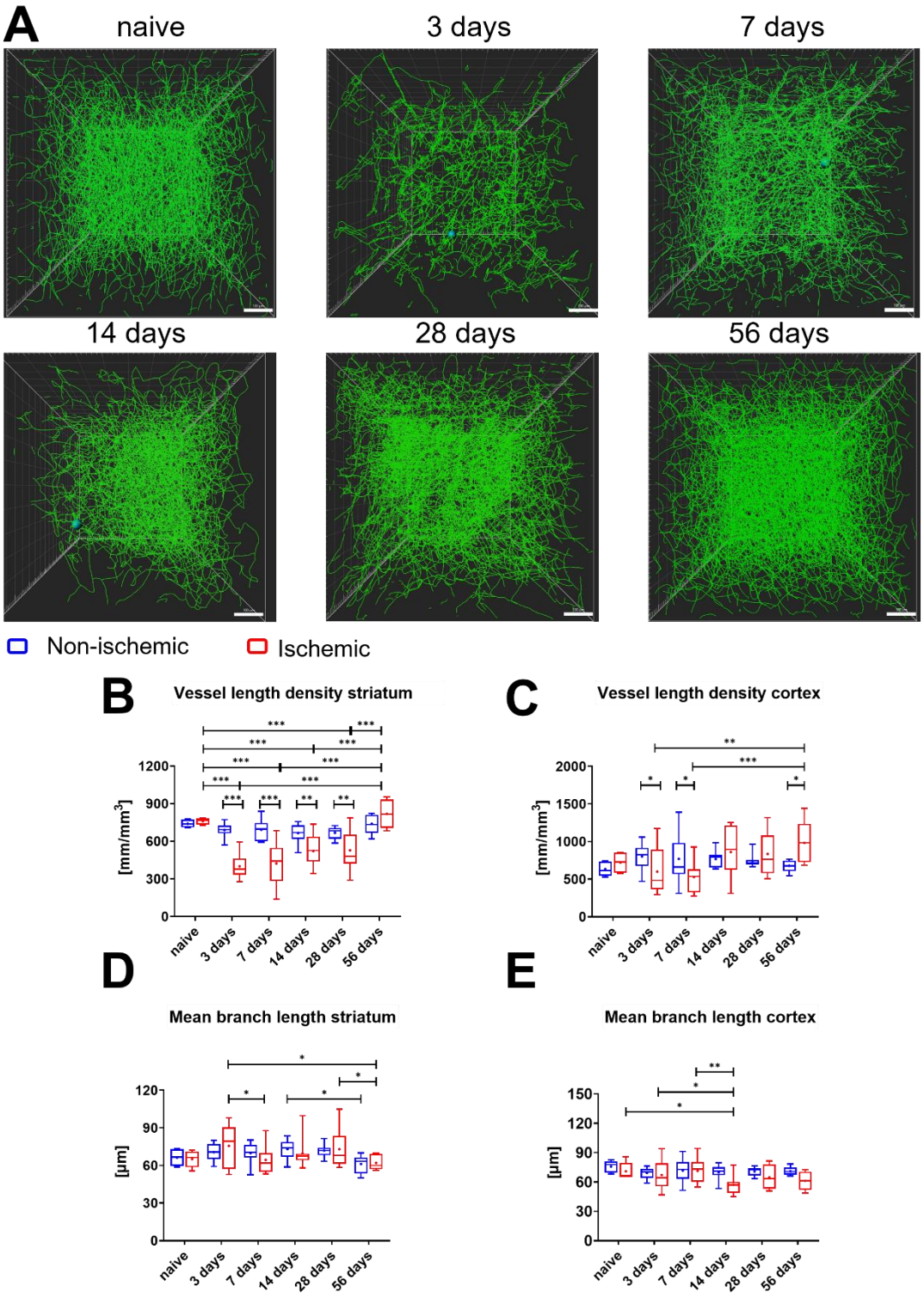

Figure 11 (for figure legend see page 31)

Figure 11. Vessel length density and mean branch length after severe stroke (Figure 11 on page 30).
Mice were subjected to 40 minutes of middle cerebral artery occlusion (MCAO) and sacrificed at the indicated time points. **A**. Images were analyzed as described above (**Fig. 10**), and representative regions from the striatum are displayed. The ROIs were processed using the Imaris filament-tracing tool. The scale bar represents 100 μm. **B and C**. Box plots displaying the length density of brain microvessels analyzed in naive animals or mice reperfused for 3, 7, 14, 28, or 56 days after 40 minutes of MCAO in the ischemic (red box) or non-ischemic (blue box) striatum or adjacent cortical areas. **D and E**. Mean branch length in the striatum and cortex were analyzed after severe ischemia at the indicated time points. Data are box plots with medians (lines inside boxes)/means (crosses inside boxes) ± interquartile ranges (IQR; boxes) with minimum/maximum values as whiskers (n=5-15 animals per group). *p<0.05, **p<0.01, ***p<0.001.

ischemia. Notably, the mean branch length was shortest in the ischemic as well as in the non-ischemic hemisphere after 56 days, the time point at which VLD was already increased after MCAO. In the cortex, the mean branch length was not altered after a mild stroke (**Fig. 10E**) but showed a slight decrease at 14 days after a severe ischemia (**Fig. 11E**).

Overall, these results suggest that VLD in the ipsilateral striatum and cortex after ischemic stroke is reduced compared to the corresponding contralateral region at the indicated early time points. However, it gradually recovers and increases, starting at 3 days after mild and severe stroke. In contrast, mean branch length tends to decrease over time, indicating that new and shorter blood vessels are formed after ischemic injury.

1.21 Vessel remodeling after mild and severe stroke

In addition to VLD and mean branch length, additional read-outs displaying vessel remodeling after stroke were analyzed. Specifically, branch density, branching point density, as well as the indirect calculation of branches/branching point were analyzed after LSFM of whole brains. Following mild stroke, the ipsilateral striatal branch and branching point densities did not differ during the first 24 hours **(Fig. 12B, C)**. Three days after both mild and severe stroke, the ipsilateral striatal branch and branching point densities decreased to their lowest values **(Figs. 12B, 12C, 13B, and 13C)**. Fifty-six days

post mild stroke, the ipsilateral striatal branch density and branching point density significantly increased compared with 3 days (p=0.0016, p=0.0006 respectively) Compared to 56 days post-stroke, the densities at all referenced time points from day 3 onward were lower. From days 3−28, the ipsilateral striatal branch and branching point densities of the ischemic striatum were consistently lower than those of the contralateral hemisphere; this condition was reversed on day 56 **(Figs. 12B, 12C, 13B, and 13C)**.

Although the nadirs of the ipsilateral cortical branch and branching point densities occur on day 3 post-mild stroke, these densities decreased at 3 hours post-ischemia compared with the naive group, slightly rising again at 24 hours **(Fig. 12E, 12F)**. Despite this initial decrease in the ipsilateral cortical branch and branching point density, they exceeded the corresponding density in the contralateral cortex at day 14 post-mild stroke, which differed from the situation in the striatum **(Fig. 12E, 12F)**. The changes in ipsilateral striatal branch and branching point densities differed after severe stroke compared to those after mild stroke. The nadirs of these densities in the ipsilateral cortex occurred 7 days after severe stroke, and an increase was observed between days 28 and 56 **(Fig. 13E, 13F)**. Although the branching point density of the ischemic cortex exceeded that of the non-ischemic cortex after both mild and severe stroke, a notable rise in that of the ipsilateral cortex compared to the contralateral cortex at day 56 was observed only after severe stroke **(Figs. 12E, 12F, 13E, and 13F)**.

The analysis of branches/branching points revealed clear differences between non-ischemic and ischemic hemispheres, both in the striatum and the cortex **(Fig. 12D, 12G)**. Specifically, the number of branches per branching point was significantly higher in the ipsilateral striatum than in the contralateral striatum in the acute to subacute phase after MCAO and reached baseline levels on days 28 and 56 post mild stroke and on day 56 post severe stroke **(Fig 12D, 13D).** Figure **12G** shows that the number of branches/branching point in the cortex does not change consistently **(Fig. 12G)**. Following severe stroke, the number of branches/branching point increased compared to non-ischemic striatum after 3, 7 and 14 days and is insignificantly changed after 28 and 56 days post severe ischemia **(Fig. 13D)**. Furthermore, an increase of branches per branching point can be observed in the ischemic cortex compared to non-ischemic tissue after severe stroke. This value consists until day 28 post-stroke **(Fig. 13G)**. However, the

analysis of branches/branching point is an indirect method that does not consider the possible impact of disrupted or blocked vessels. Therefore, this data should be carefully interpreted.

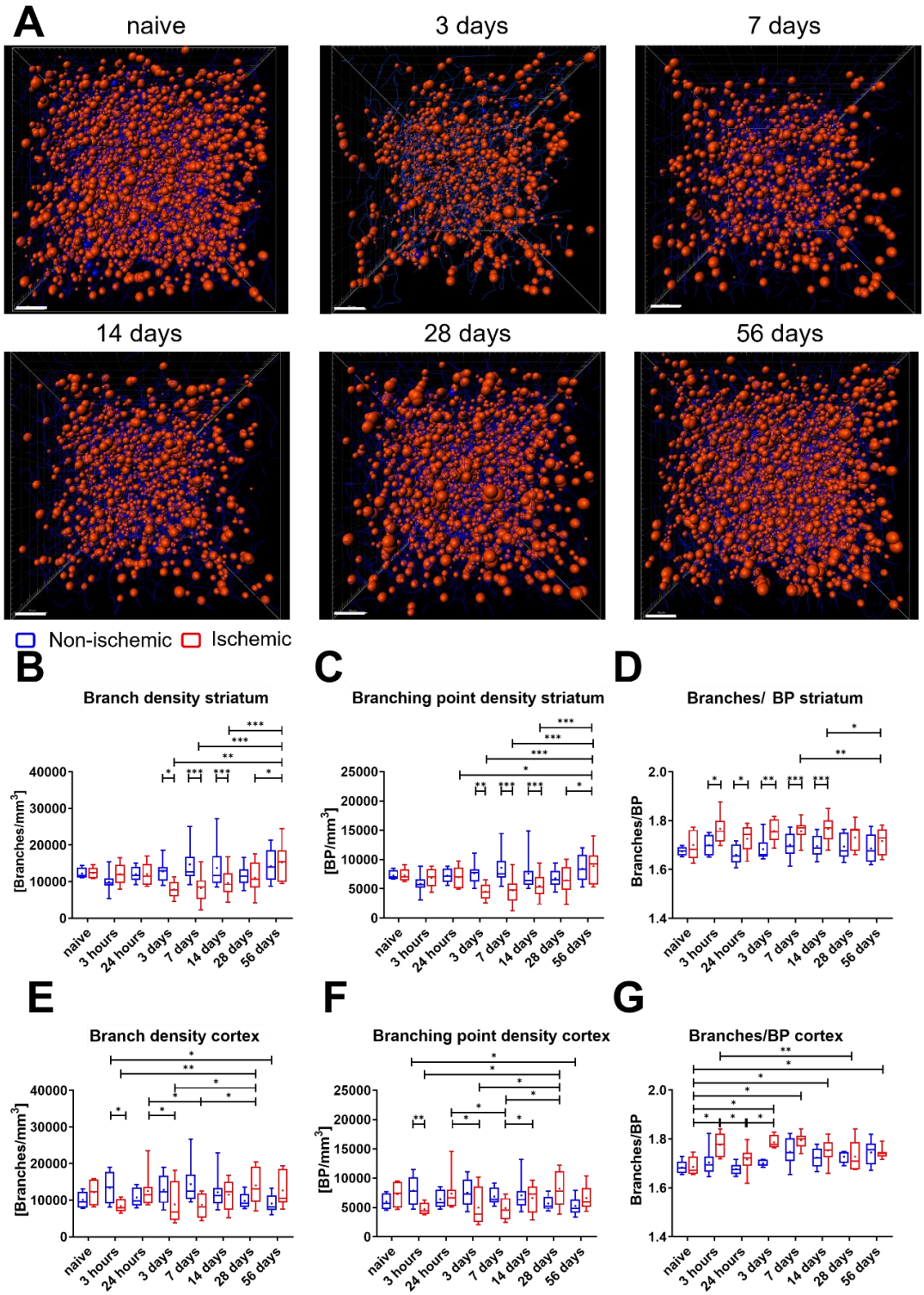

Figure 12 (for figure legend see page 34)

Figure 12. Reorganization of cerebral branches post-mild stroke (Figure 12 on page 33)

A. Representative images of branching points (BPs) in striatal regions in the center of the core region in the ipsilateral hemisphere after mild stroke processed using the Imaris filament-tracing tool. Branch and BP densities were calculated from the number of branches or BPs per mm^3, whereas branches/BP was calculated as the number of branches per BP, respectively. The scale bars represent 100 μm**.** Box-plots show branch density (**B**), branching point density (**C**) and branches/BP (**D**) of cerebral microvessels analyzed in naïve animals or mice subjected to 20 minutes of middle cerebral artery occlusion (MCAO) followed by reperfusion for 3 or 24 hours, and at 3, 7, 14, 28, or 56 days in the ischemic (red boxes) or non-ischemic (blue boxes) striatum. branch density (**E**), branching point density (**F**) and branches/BP (**G**) of cerebral microvessels analyzed at the indicated time points after mild ischemia in the cortex. Data are box plots with medians (lines inside boxes)/means (crosses inside boxes) ± interquartile ranges (IQR; boxes) with minimum/maximum values as whiskers *p<0.05, **p<0.01, ***p<0.001 (n=5-15 animals per group).

1.22 Variation in vascular tortuosity after mild and severe stroke

As the VLD, branching point density, and mean vessel diameter changed after stroke, we subsequently studied whether the tortuosity of the vessels played a vital role during angiogenesis after stroke. Figure **14A** represents vessel tortuosity at the indicated time points, with less tortuous vessels indicated toward the red end of the spectrum (an index close to 1) and more tortuous vessels indicated toward the blue end of the spectrum (a larger tortuosity index). There was no difference in tortuosity expressed as the reciprocal of straightness up to 56 days post-mild stroke between the non-ischemic and ischemic hemispheres. On day 56 after 20 minutes of MCAO, the striatal vessel tortuosity had slightly increased (p=0.0351) compared with that on day 7 (**Fig. 14B)**. However, in the cortex, vessels were the straightest on day 3 with an increase compared with 3 days in tortuosity on days 14 (p=0.0039), 28 (p=0.0286), and 56 (p=0.0005) **(Fig. 14C)**. Tortuosity was lower on days 3 (p=0.0048) and 7 (p=0.0093) compared to the naive group.

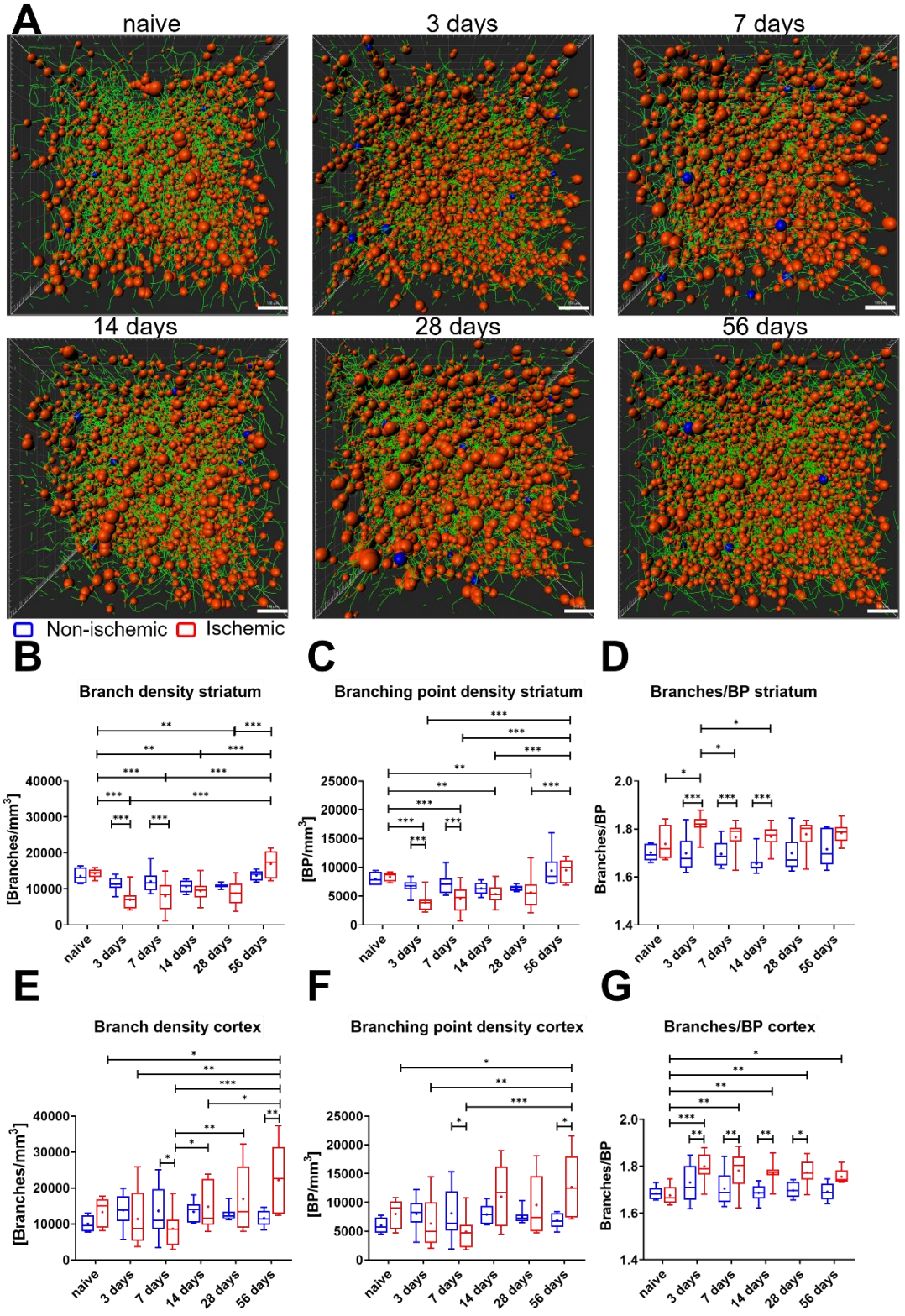

Figure 13 (for figure legend see page 36)

Figure 13. Reorganization of cerebral branches after severe stroke (Figure 13 on page 35)

A. Images of striatal regions in the core region of the ipsilateral hemisphere processed using the Imaris filament-tracing tool with branching points (BPs) displayed in orange. Scale bars represent 100 μm. Box plots show branching density (**B**), branch point density (**C**), and branches/BP (**D**) of cerebral microvessels were analyzed in naive animals or in mice subjected to 40-minute middle cerebral artery occlusion (MCAO) after reperfusion for 3, 7, 14, 28, or 56 days in the ischemic (red boxes) or nonischemic (blue boxes) striatum. **E**, **F**, and **G** Branch density (**E**), branch point density (**F**), and branches/BP (**G**) of cerebral microvessels analyzed after the indicated time points following severe ischemia in the ischemic cortical region. Data are box plots with medians (lines inside boxes)/means (crosses inside boxes) ± interquartile ranges (IQR; boxes) with minimum/maximum values as whiskers *p<0.05, **p<0.01, ***p<0.001 (n=5-15 animals per group).

Fig. 15A represents the tortuosity of vessels after severe stroke. The variation in tortuosity following severe stroke was lower in the striatum than in the cortex. Compared to the naive group, there was a decrease in tortuosity on days 3 (p=0.0257) and 7 (p=0.0126), and the tortuosity increased on day 56 compared with those on days 3 (p=0.0029), 7 (p=0.0009), 14 (p=0.0414), and 28 (p=0.0121) post-severe stroke (**Fig. 15B)**. On day 7, the tortuosity of vessels in the ipsilateral striatum was lower than that in the contralateral hemisphere (**Fig. 15B)**. However, following a severe stroke, vessel tortuosity in the cortex decreased to its nadir at day 7 (p=0.0020), after which it increased compared with 7 days at days 14 (p<0.0001), 28 (p=0.0003), and 56 (p<0.0001) (**Fig. 15C)**.

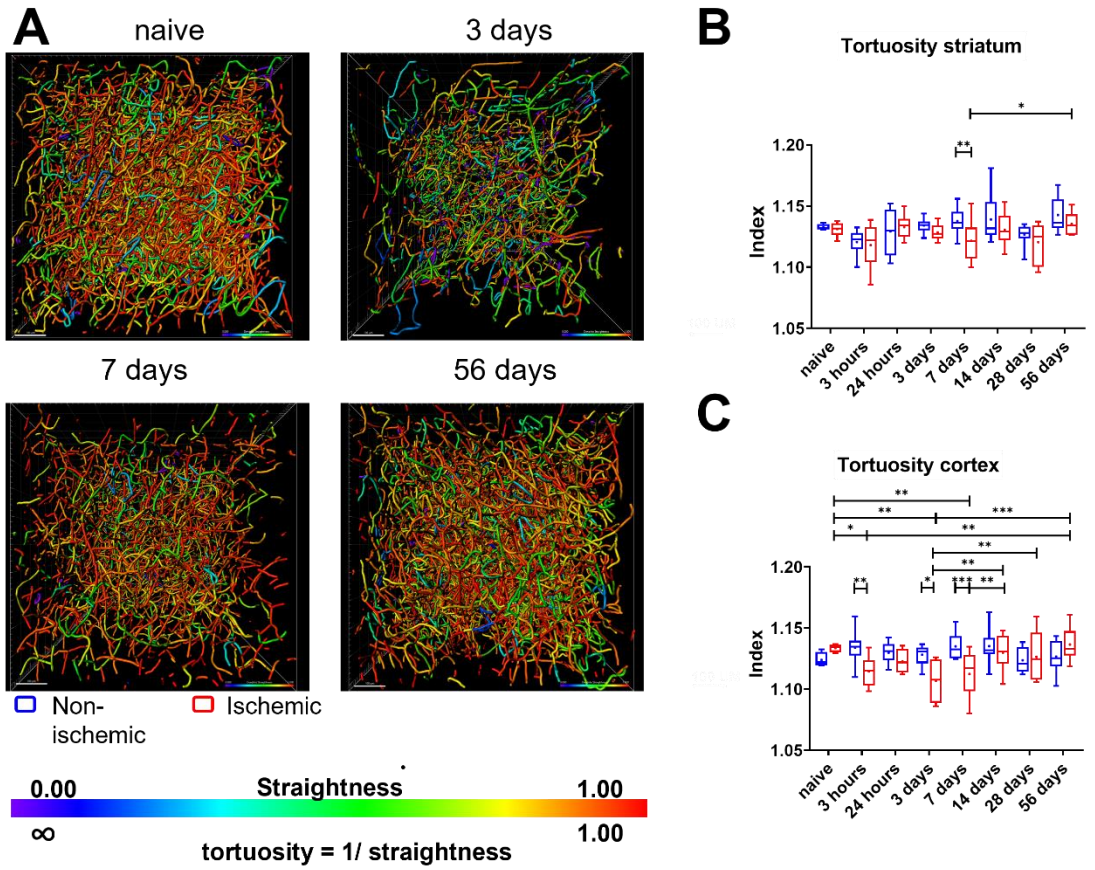

Figure 14. Tortuosity of vessels in mice after mild stroke

A. The images were processed using Imaris software. Straightness was defined by the filament-tracing algorithm in imaris and tortuosity was calculated by 1/striaightness. Scale bars represent 100 μm, and the spectrum bar represents dendrite straightness 0.000−1.000 as displayed in imaris software. Vessels toward the blue end of the spectrum are infinitely tortuous, which was labeled as ∞, and those toward the red end of the spectrum are straighter which was labeled as 1.00 under the spectrum bar. Images represent striatal regions in the core region of stroke from naive brains to day 56 after mild stroke. **B and C**. Box-plots show tortuosity of cerebral microvessels analyzed in naïve animals or mice subjected to 20 minutes of middle cerebral artery occlusion (MCAO) followed by reperfusion for 3 or 24 hours, and at 3, 7, 14, 28, or 56 days in the ischemic (red boxes) or non-ischemic (blue boxes) striatum (**B**) or the adjacent cortical region (**C**) Data are box plots with medians (lines inside boxes)/means (crosses inside boxes) ± interquartile ranges (IQR; boxes) with minimum/maximum values as whiskers *p<0.05, **p<0.01, ***p<0.001 (n=5-15 animals per group).

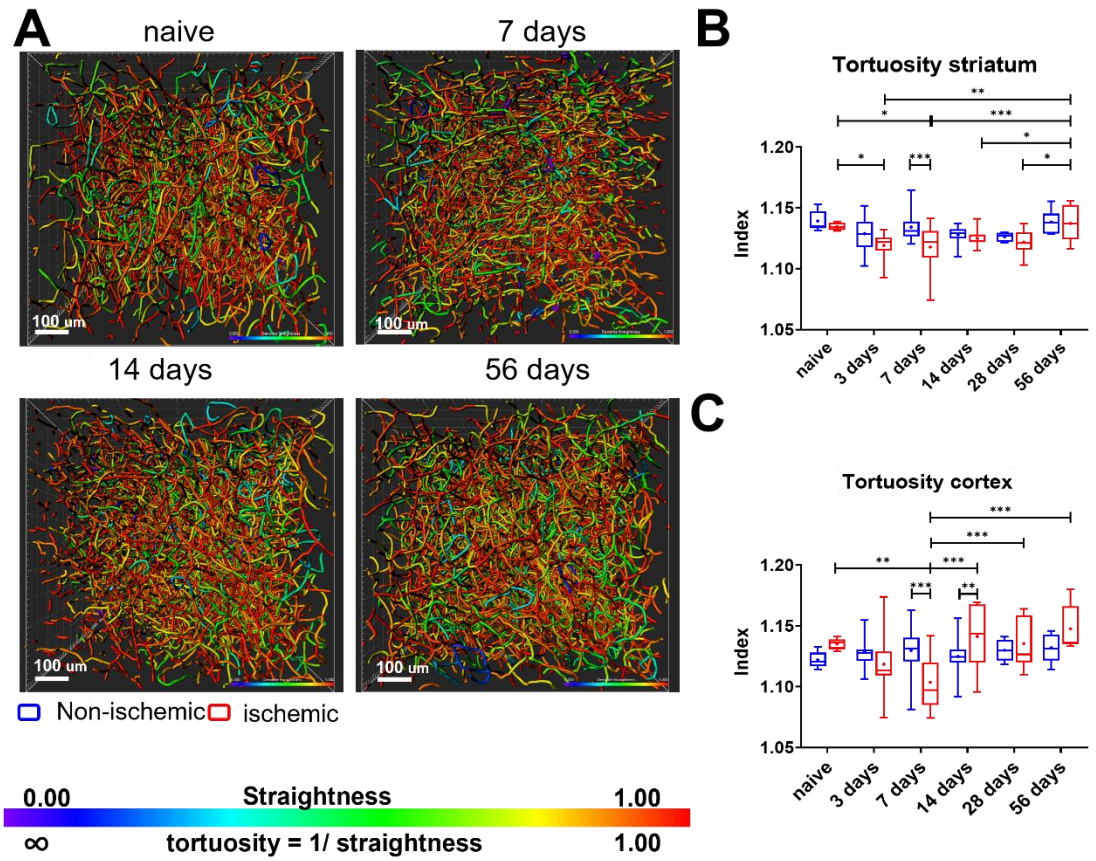

Figure 15. Tortuosity of vessels in mice after severe stroke

A. The images were processed using Imaris software. Straightness was defined by the filament-tracing algorithm in imaris and tortuosity was calculated by 1/striaightness. Scale bars represent 100 µm, and the spectrum bar represents dendrite straightness 0.000−1.000 as displayed in imaris software. Vessels toward the blue end of the spectrum are infinitely tortuous, which was labeled as ∞, and those toward the red end of the spectrum are straighter which was labeled as 1.00 under the spectrum bar. Representative images of striatal regions in the core region of stroke from naive brains to day 56 after severe stroke. **B and C**. Box-plots show tortuosity of cerebral microvessels analyzed in naïve animals or mice subjected to 40 minutes of middle cerebral artery occlusion (MCAO) followed by reperfusion at 3, 7, 14, 28, or 56 days in the ischemic (red boxes) or non-ischemic (blue boxes) striatum (**B**) or the adjacent cortical region (**C**). Data are box plots with medians (lines inside boxes)/means (crosses inside boxes) ± interquartile ranges (IQR; boxes) with minimum/maximum values as whiskers *p<0.05, **p<0.01, ***p<0.001 (n=5-15 animals per group).

1.23 hanges in infarct area and volume after FTY720 treatment

To verify that the autofluorescence signal using LSFM is suitable to analyze infarct volumes after mild and severe ischemia, mice were treated for 7 or 14 days post-stroke after 20 or 40 minutes of MCAO with FTY720 starting at day 1 after surgery. This drug is a well-established therapeutic agent used in multiple sclerosis treatment and was already shown to be protective in experimental stroke treatment (Kraft, et al., 2013). Images were obtained with LSFM based on the tissue autofluorescence to analyze the surface area and volume of the infarct using the Imaris volume and surface tools as described above. at days 7 and 14 after mild and severe ischemia followed by daily treatment with 1 mg/kg FTY720 or vehicle starting on day 1 post-ischemia **(Fig. 16A, 17A)**. The autofluorescence signal indicated that mice treated with FTY720 following 20 minutes of ischemia displayed a similar infarct volume and surface area at both days 7 and 14 as mice receiving only the vehicle **(Fig. 16B, 16E)**. However, 7 days after a severe stroke, mice treated with FTY720 showed a significant reduction in infarct volume ($p=0.0012$) and surface area ($p=0.0008$) compared to mice receiving vehicle **(Fig. 17B, 17C)**. However, after 14 days, only the infarct surface area was statistically decreased in mice treated with FTY720 compared to mice treated with vehicle ($p=0.0127$) **(Fig. 17D)**, whereas the infarct volume showed no noticeable changes between mice treated with FTY720 or vehicle ($p=0.1100$) **(Fig. 17E)**.

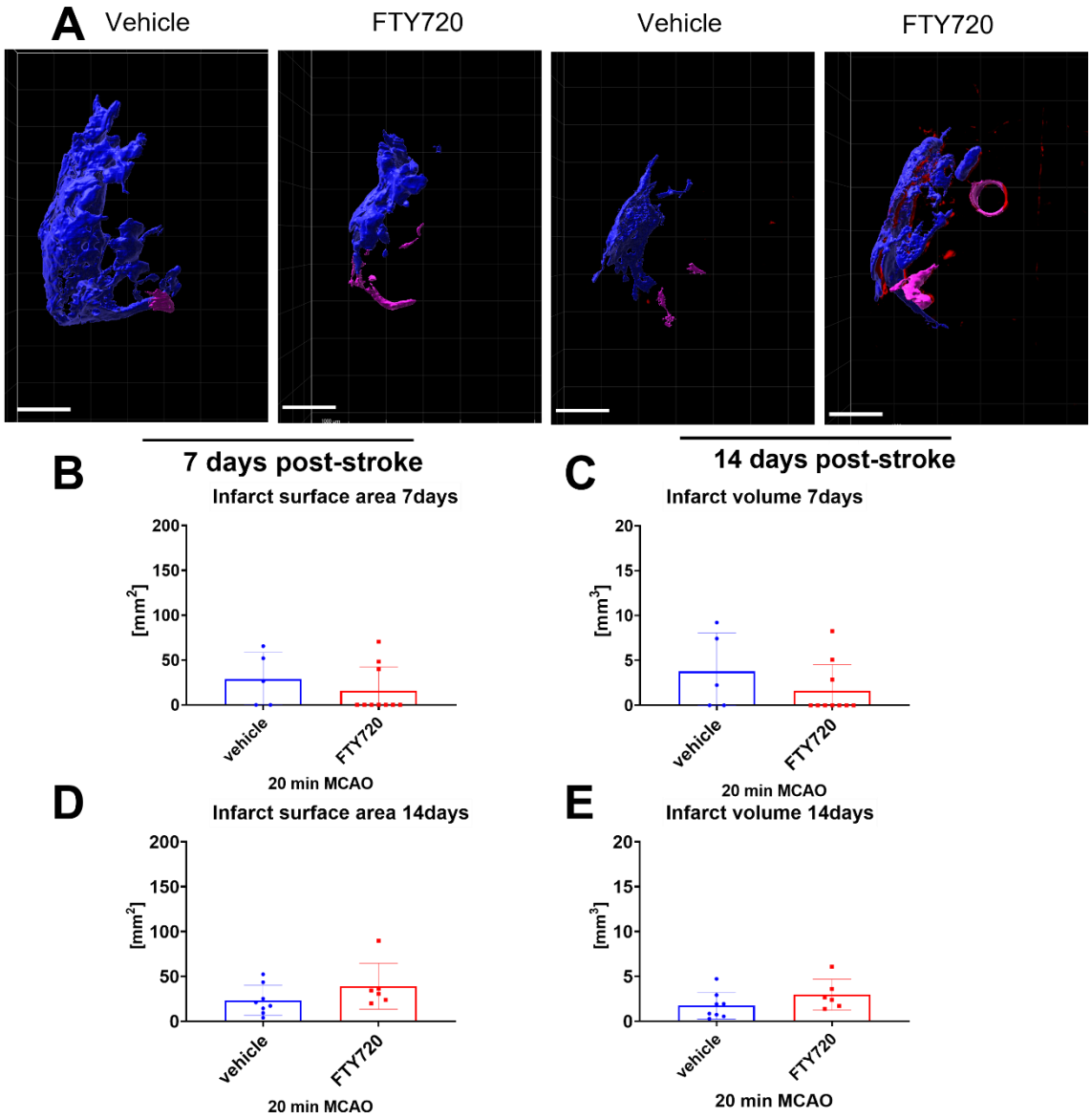

Figure 16. Infarct surface area and volume in mice receiving FTY720 treatment after 20 minutes of MCAO

A. Representative images of brain infarct volume measurement in brains obtained 7 and 14 days after 20 minutes of ischemia followed by vehicle or FTY720 treatment. Autofluorescence of tissue using light-sheet fluorescence microscopy (LSFM) was detected to analyze infarcts using Imaris volume and surface tools. Scale bars represent 1000 µm. B-E. Box-plots show infarct volume and surface area analyzed in the FTY720-treated group and vehicle animals subjected to 20 minutes of middle cerebral artery occlusion (MCAO) followed by reperfusion after 7 or 14 days. *p<0.05, **p<0.01, ***p<0.001.(n=5-10 animals per group)

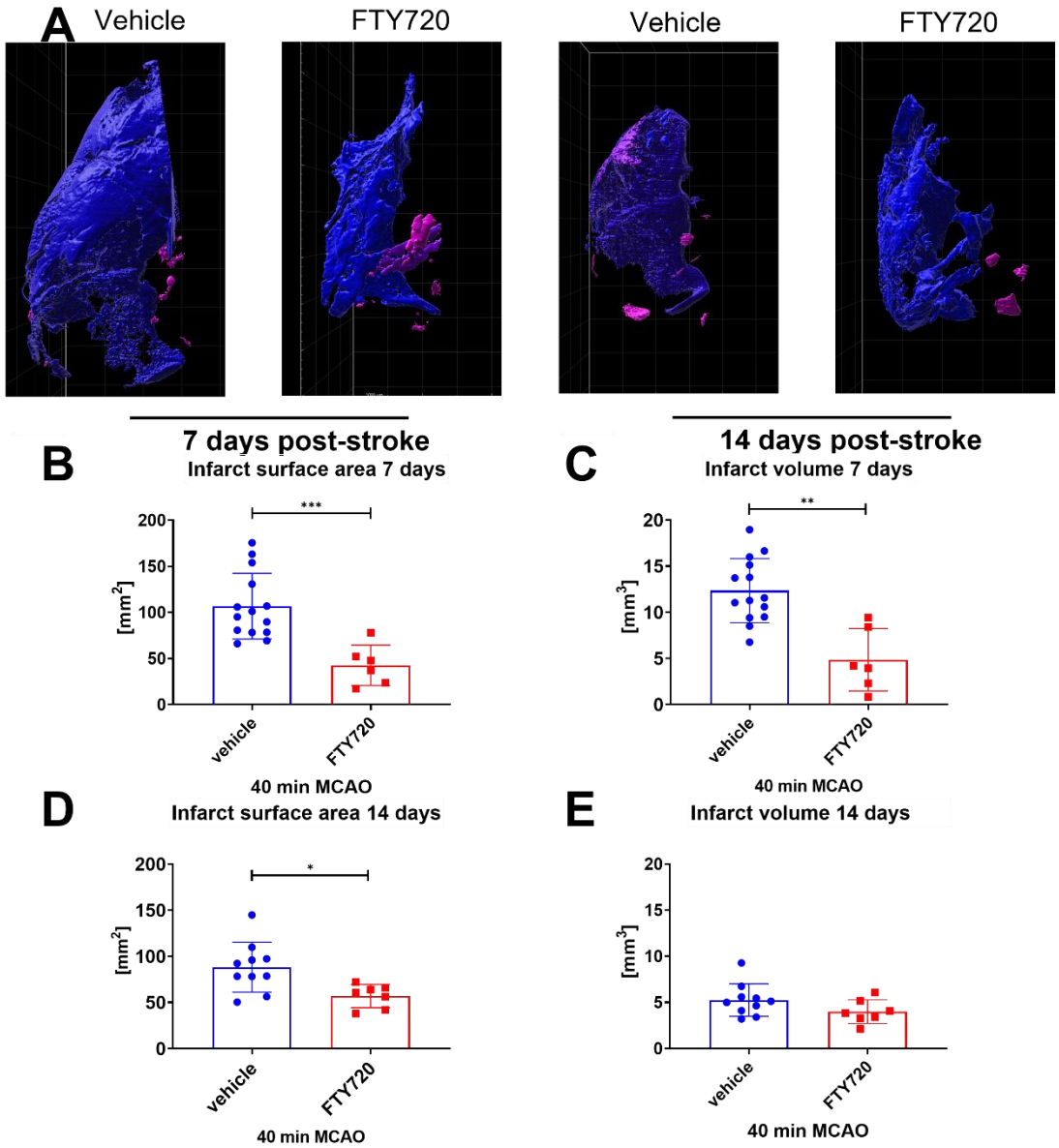

Figure 17. Infarct surface area and volume in mice receiving FTY720 treatment after 40 minutes of MCAO

A. Representative light-sheet fluorescence microscopy (LSFM) images of brain infarct volume in brains obtained 7 and 14 days after 40 minutes of ischemia in vehicle and FTY720 treatment groups, respectively. Autofluorescence of tissue was detected to analyze infarcts using Imaris volume and surface tools. The scale bar represents 1000 µm. **B-E**. Box-plots show Infarct volume and surface area analyzed in the FTY720-treated group and vehicle animals subjected to 40 minutes of middle cerebral artery occlusion (MCAO) followed by reperfusion after 7 and 14 days. *p<0.05, **p<0.01, ***p<0.001 (n=6−14 animals per group).

1.24 Vascular remodeling upon treatment of mice with FTY720 revealed by LSFM

High-resolution images of FITC-albumin labeled blood vessels were obtained with LSFM in the striatum and adjacent cortex for analysis of angiogenesis using the Imaris filament tool as described above at day 7 and day 14 after mild and severe ischemia followed by treatment with vehicle or the S1P receptor modulator FTY720. Compared with the contralateral hemisphere, vessel length and BP density in the ipsilateral striatum were lower in both vehicle and FTY720-treated mice on day 7 after mild stroke. However, on day 14, VLD in the ischemic hemisphere of FTY720-treated animals was significantly increased compared to the vehicle group. **(Fig. 18B, 18C)**. In the cortex, VLD density was similarly increased after 14 days of FTY720 treatment compared to the vehicle treated group, whereas BP density was not significantly altered upon FTY720 treatment **(Fig. 18D, 18E)**.

After severe stroke, vascular length and BP density were lower in the ipsilateral striatum in both vehicle-treated and FTY720-treated mice compared to the contralateral hemisphere after 7 days. However, 14 days after a severe stroke, mice receiving FTY720 had significantly higher VLD and BP density in the ischemic hemisphere than those receiving vehicle treatment **(Fig. 19B, 19C)**. In contrast, VLD and BP density in the cortical regions was not affected significantly by FTY720 treatment, neither at 7 nor at 14 days post-ischemia. **(Fig. 19D, 19E)**.

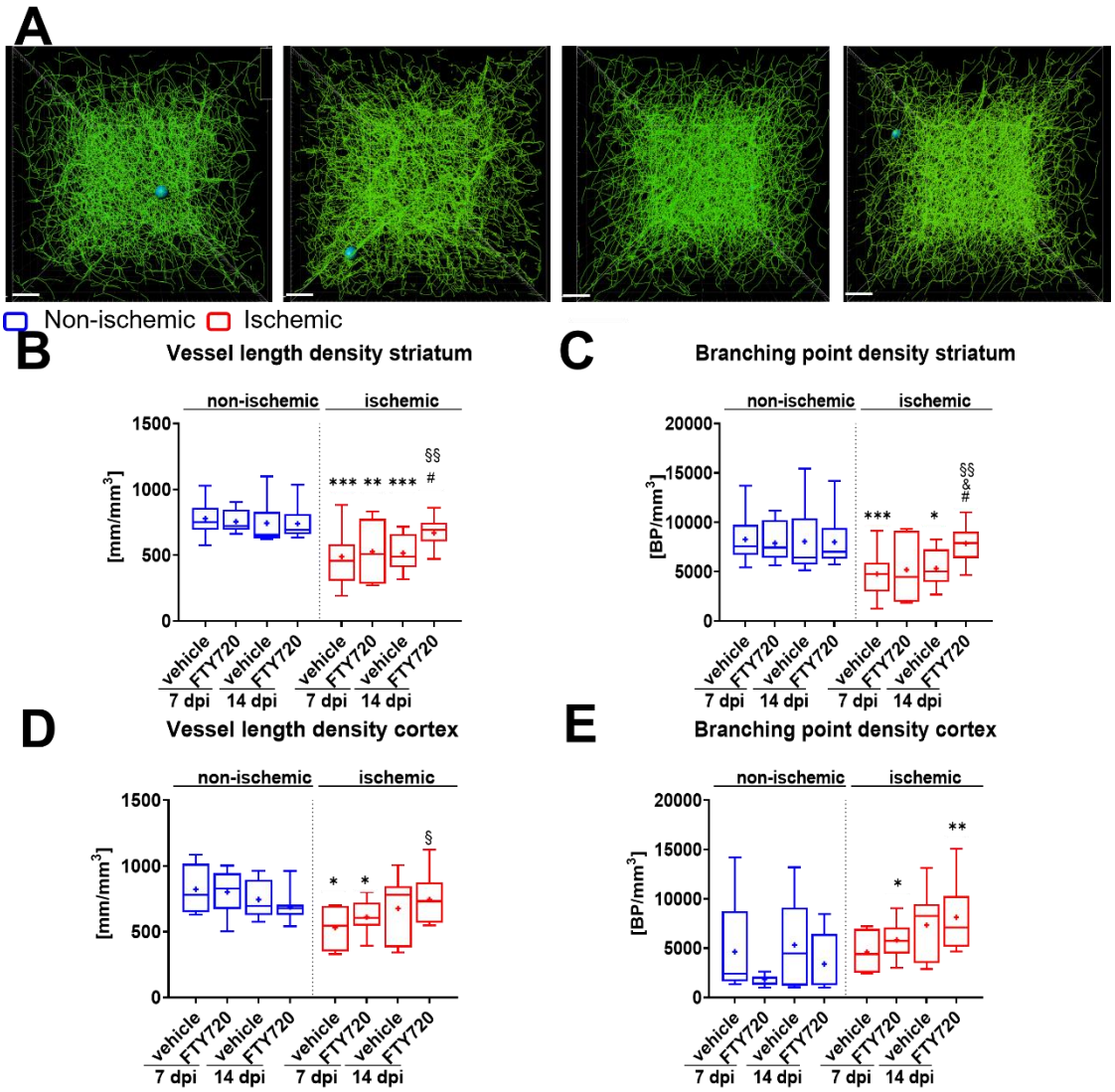

Figure 18. Influence of FTY720 treatment on microvascular reorganization after mild stroke

A. Representative images processed using the Imaris filament-tracing tool. Analysis of striatal and cortical vessel length and branching point density in brains of mice subjected to 20 minutes of ischemia followed by treatment with 1 mg/kg FTY720 (or vehicle only), starting 1 day post-ischemia for 7 or 14 days before perfusion with FITC-conjugated albumin-containing hydrogel. The scale bars represent 100 µm. **B and D** Box-plots show vessel length density (VLD) of cerebral microvessels analyzed in the FTY720-treated group and vehicle animals subjected to 20 minutes of MCAO followed by reperfusion after 7 or 14 days in the ischemic (red boxes) or non-ischemic (blue boxes) striatum (**B**) or the adjacent cortical region (**D**). **C and E** Box-plots show branching point density of cerebral microvessels analyzed in the FTY720-treated group and vehicle animals subjected to 20 minutes of middle cerebral artery occlusion (MCAO) followed by reperfusion after 7 or 14 days in the ischemic (red boxes) or non-ischemic (blue boxes) striatum (**C**) or the adjacent cortical region (**E**). * / ** / *** $p<0.05$ / 0.01 / 0.001 vs. corresponding non-ischemic hemisphere. § $p<0.05$ vs. vehicle at 7 dpi. # $p<0.05$ vs. vehicle only at 14 dpi. days post-ischemia. BP, branching points.

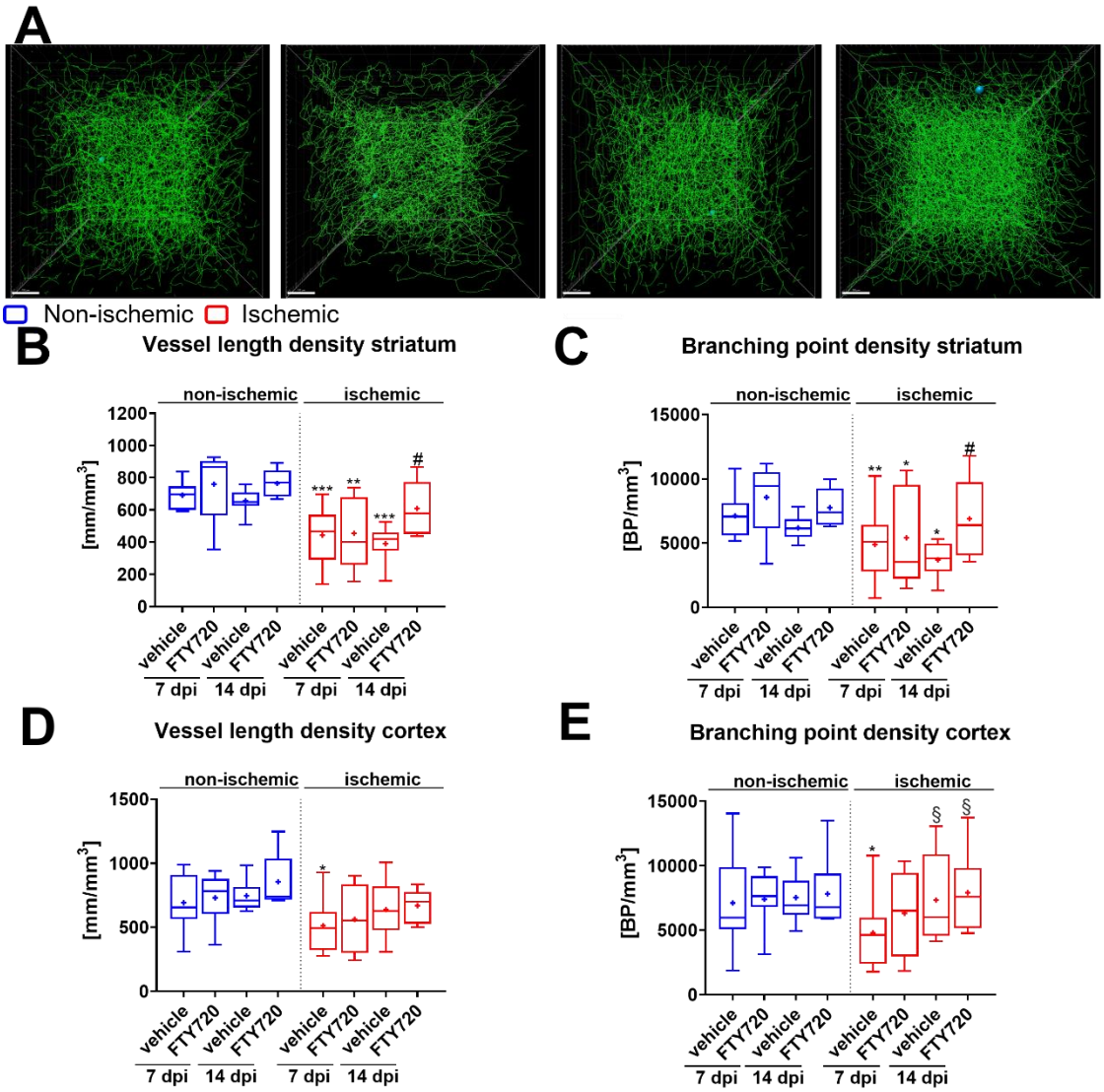

Figure 19. Influence of FTY720 treatment on microvascular reorganization after severe stroke

A. Representative images processed using the Imaris filament-tracing tool. Analysis of striatal and cortical vessel length and branching point density in brains of mice subjected to 40 minutes of ischemia followed by treatment with 1 mg/kg FTY720 (or vehicle only), starting 1 day post-ischemia for 7 or 14 days before perfusion with FITC-conjugated albumin-containing hydrogel. The scale bars represent 100 µm. **B and D** Box-plots show vessel length density (VLD) of cerebral microvessels analyzed in the FTY720-treated group and vehicle animals subjected to 40 minutes of middle cerebral artery occlusion (MCAO) followed by reperfusion after 7 or 14 days in the ischemic (red boxes) or non-ischemic (blue boxes) striatum (**B**) or the adjacent cortical region (**D**). **C and E** Box-plots show the branching point density of cerebral microvessels analyzed in the FTY720-treated group and vehicle animals subjected to 40 minutes of MCAO followed by reperfusion after 7 or 14 days in the ischemic (red boxes) or non-ischemic (blue boxes) striatum (**C**) or the adjacent cortical region (**E**). * / ** / *** $p<0.05$ / 0.01 / 0.001 vs. corresponding non-ischemic hemisphere. § $p<0.05$ vs. vehicle at 7 dpi. # $p<0.05$ vs. vehicle only at 14 dpi. days post-ischemia. BP, branching points.

DISCUSSION

Within this study, we investigated vascular reorganization following mild and severe tMCAO using fluorescence-based 3D LSFM, followed by selecting ROIs and creating Frangi filters, which were subsequently imported into Imaris software for analysis. In parallel, we utilized a bright autofluorescent signal evoked by ischemia to estimate the volume of cerebral infarction and tissue autofluorescence of examined striatum volume as well. The study revealed numerous details of the vasculature, revealing new perspectives of vascular reorganization that have hitherto not been seen as accessible

In order to investigate the concept of microvascular remodeling as a treatment for stroke, the knowledge of VLD is required. In previous studies, authors found that the number of vessels significantly increased as early as 1 day until 21 days after the stroke in mice using a complementary DNA (cDNA) array method as well as Western blotting (Hayashi et al., 2003) This result is consistent with our study. Moreover, the details of branching, including the branch density, branching point density and branches/BP, in the cortex and striatum were studied here as well. These parameters show pronounced changes after 3 days post-ischemia, reflecting decreased VLD, branch density and branching point density, which was partially or fully restored after 28 to 56 days, depending on the stroke severity. Hence 3D imaging can be used to measure the branching morphology instead of merely measuring collateral hemodynamic changes. A previous study suggested that, after stroke, the early increase of cerebral blood volume (CBV) may result from the opening of pre-existing branches. The late phase of CBV increase may be due to angiogenesis (Lin et al., 2008). Therefore, BPs also represent revascularization, which supports the results of this study. Even at 56 days after stroke, the branching point density continued to grow. VLD increased from 3 to 56 days after stroke in mice as well. However, previous studies have quantified vessel length in thin or thick histological sections (Tsai et al., 2009; Boero et al., 1999) or using staining of endothelial cells that surround the infarct area as early as 12-24 hours afterwards. An increase in vascularity in the peri-infarct region 3 days after ischemic injury was detected (Beck et al., 2000, Marti et al., 2000), but the authors drew conclusions without showing more details. Our study allows visualization of many vascular details in a 3D structure, allowing assessment of changes

in vessel density and branching. Nevertheless, as hydrogel labeling is based on the flow of blood, non-perfused vessels cannot be labeled with the method used in this study..

Most researchers studying cerebral vasculature by conventional histochemistry elucidated microvascular remodeling and angiogenesis only up to 28 days post-stroke. However, in 2007, Lyden and colleagues proposed a “clear-up hypothesis”, whereby newborn vessels disappear while removing cellular debris from pan-necrotic tissue, suggesting that post-stroke brain angiogenesis is transient rather than permanently involved in neuronal recovery. They illustrated that the length and density of microvessels after 30 days was statistically significantly larger in the ischemic than in the non-ischemic hemisphere. This difference was abated partially by day 90 and entirely by day 165 after tMCAO. Those results are not in conflict with the results from this present study, wherein the VLD and BPs still seemed to be increasing at 56 days after the stroke, however, the ipsilateral values were never higher than the contralateral values or at least did not exceed them to a relevant extent, which has not been reported up to this point. These previous researchers employed immunohistochemistry (Manoonkitiwongsa et al., 2001, Yu et al., 2007), whereas 3D visualization was used in our study, which enables vascular network reconstruction and analysis. Conventional histochemistry allows evaluating small vessel segments, while we provided an unbiased analysis of vascular networks in defined brain areas

Microvessels in an infarct area are frequently coiled into a cavity where brain parenchyma has been lost. These tortuous vessels and cavities were referred to as tortuous lesions in this study. Tortuosity increases a vessel’s length, accompanied by a loss of kinetic energy for each turn and loop (Brown et al., 2011). The arterioles typically become more tortuous in individuals aged between 60 and 70 years (Hassler et al., 1967). According to previous studies, alterations in blood flow and pressure are one of the factor of vascular tortuosity, whereas arterial dynamics, buckling and vessel wall remodeling contribute to the development of vascular tortuosity, which explains why increased tortuosity can be observed after stroke (Han, 2012). Vessels with multiple branching points are more likely to form a series of small loops than a large conduit with no branches, taking the shape of a single loop or a simple “S” shape, and vessels with large diameters require a longer path length to generate tighter angles compared to smaller vessels (Ciurică et al., 2019). Hence,

when studying angiogenesis by measuring tortuosity, additional details of the vascular networks are provided. The results of this study demonstrate that the branching points differed the most between the ipsilateral and contralateral striata at 7 days post-stroke, with fewer branching points in the ipsilateral striatum. From 28 days onward, the branching-point density, vessel diameter, and tortuosity did not differ between the ipsilateral and contralateral striata, which indicates that the remodeling of the vasculature is more stable in the later phases after stroke. This result is supported by those from several previous studies (Xiong et al., 2010; Popa-Wagner et al., 2010; Slevin et al., 2006).

Additionally, based on our time course studies of microvascular remodeling, we investigated the influence of the S1P receptor modulator FTY720 treatment on vascular angiogenesis in mild and severe stroke by measuring VLD and branching point density after 7 and 14 days, respectively. FTY720 exhibits potent activity in neurons, glial cells, and brain microvascular endothelial cells (Billich et al., 2003; Blondeau et al., 2007). Tian reported in 2020 that FTY720 can promote angiogenesis in the ischemic zone after photothrombotic stroke, a type of stroke that mimics a cortical stroke, which they determined by using CD31 + BrdU staining at day 14 post-stroke. Their results were in line with those of this study, The VLD significantly increased 14 days after stroke in FTY720-treated mice compared to the vehicle group. Our research is supported by another study carried out by Malone in a permanent MCA distal occlusion mice model, which showed the most evident effect was noted when the mice were treated with FTY720 for 10 days after ischemia with a significant increase in the number of FoxP3+ cells in the infarct core (Malone et al., 2021). FoxP3+ cells are the most important molecular marker of regulatory T cells and are found to be expressed in excess in all regulatory T cells. In our model, VLD and BP density in FTY720-treated mice increased considerably at day 14 post-stroke, whereas no significant increase of VLD and BP density was detected at 7 days post-stroke. Therefore, we hypothesize that the observed effects are more likely related to the initiation of angiogenesis than to the protection of vessels by FTY720 after stroke. S1P receptor 1 on endothelial cells is able to sense shear stress and transduce its signaling pathway triggering the development of collateral vessels in ischemic stroke (Iwasawa et al., 2018). Such collateral recruitment is strongly correlated with the sprouting of the main stem, which may account for the more pronounced increase in branching point density than VLD in this study (Liu et al., 2014). Our study provides

evidence for the first time that the cortical region adjacent to the stroke undergoes vascular remodeling after stroke, resulting in significantly increased VLD with the use of FTY720 for 14 days. To date, most of the results presented by investigators for the treatment of stroke with FTY720 have been positive, however, they have not discriminated between the degree of stroke, and we found that FTY720 was equally efficient after a mild stroke as it is after severe ischemia, which will provide new insights into the immune response and treatment after stroke.

As the ischemia was located in the MCA territory and the area of infarct included both cortical and subcortical tissues, we used the infarct surface area as an auxiliary measure to evaluate the accuracy of our findings. In brain lesions, volume and surface area are two parameters of relevance. Revealing a diverse aspect of the morphology of the infarct (Gautam et al., 2015). Infarct size and brain striatal volume were analyzed using 3D reconstruction based on intensive autofluorescence and tissue autofluorescence, respectively. Previously, infarct volume was mainly determined with computed tomography, magnetic resonance imaging (MRI), and/or histology of brain sections, followed by reconstruction of the infarct volume of the brain tissue as an imaging stack (Lin et al., 1993; NINDS, 2000) and evaluation of the critical value. TTC-staining is the gold standard for infarct visualization and can be used up to 3 days post-tMCAO; Nissl or hematoxylin staining was commonly used when more than 3 days had elapsed since the stroke (Türeyen et al., 2004). However, the detection of autofluorescence cannot be used to estimate the infarct volume less than 3 days post-stroke because autofluorescence can be produced by many endogenous fluorophores during brain injury (Pascu et al., 2009). Since necrosis of neurons begins at 6 h after arterial occlusion, endogenous fluorophores are released. The edges of the necrotic tissue may become clearly demarcated after 4 to 5 days of arterial occlusion (Garcia et al., 1995). Above all, the volume obtained after 7 days post-stroke is more reliable whereas at time points later than 14 days post mild stroke, the infarcted tissue has presumably already cicatrized. In a previous study, measurement of infarct volume from autofluorescence showed comparable results when compared to Nissl staining after 7 days of ischemia (Mohamud Yusuf et al., 2021).

Since infarct volume is directly related to the outcome of ischemic stroke, we studied the effect of FTY720 (a known S1P receptor agonist) on severe and mild stroke using the same approach, and the results clearly demonstrated that FTY720 could reduce infarct size and volume 7 or even 14 days after severe infarction. Previously, different effects were reported for FTY720 when it was used to treat relapsing multiple sclerosis by sequestering lymphocytes in the lymph nodes and preventing them from contributing to an anti-immune response. Because the immune system plays a crucial role in correcting the damage after a stroke, this drug was applied to treat strokes and positive results were obtained. In certain studies, FTY720 significantly decreased stroke area and improved functional outcome in wild-type mice on days 1 and 3 after tMCAO (Kraft et al., 2013); however, these previous studies focused on cortical infarcts or infarcts of moderate size, in contrast to the study performed by Liesz (Liesz et al., 2011). Furthermore, most studies were conducted between 0 and 7 days after stroke, with longer-term studies being much rarer. In the case of severe stroke (mice subjected to more than 30 minutes of tMCAO), numerous studies have demonstrated that the infarct size was reduced after FTY720 treatment, similar to the results of this study (Brait et al., 2016; Salas-Perdomo et al., 2019; Naseh et al., 2021).

Furthermore, we used the autofluorescence signal of brain tissue to measure the variations of striatal volume after a mild and severe stroke. Endogenous autofluorescence clearly showed the structure of the brain in projected coronal sections, allowing the contours of the striatum to be drawn and eventually connected to obtain the volume of the striatum using the surface tool in Imaris. When applying this method, the volume can be reliably measured at all time points after ischemia. We detected shrinkage of the ischemic striatum as early as 14 days, continuing until 56 days after the stroke (with the shrinkage of ischemic tissue being more pronounced after severe stroke). Previously, the striatal and thalamic shrinkage in the acute to chronic phases of ischemic stroke were investigated in relation to radiologically identified lesions; the shrinkage was not related to lesion size and was suggested to be independent of the ischemic event (Kraemer et al., 2004), which supports the results obtained here. The post-ischemic infarct volume decreased over time, although striatal shrinkage was more prominent. Overall, severe stroke seriously affects the striatal structure. Meanwhile, vasogenic edema, especially in the early phases after stroke onset, is more prominent after a severe stroke than after a mild stroke (Werring et

al., 2000; Kang et al., 2000). Moreover, we could show that LSFM imaging can be used to replace conventional TTC or Nissl stainings to measure infarct volume after 7 days of infarct, and the endogenous autofluorescence of brain tissue can be utilized to reliably measure swelling or shrinkage of tissue. One advantage to this being that fewer animals are needed for testing, as the very same brain can be used for different read-outs.

In summary, the applicability of LSFM was evaluated in measuring post-stroke 3D microvasculature in the mouse brain, including infarct size and angiogenesis, VLD, BPs and vascular tortuosity in the acute and chronic phases after mild and severe stroke and upon FTY720 treatment. The results of this investigation are consistent with previous studies but demonstrate additional vascular details. This is the first time that vessels have been quantified and angiogenesis has been visualized in a 3D reconstruction over a long time period post-stroke. While the study presents a promising result, there are some caveats. Larger groups of mice are required for each indicated time point. During our analyses, we were encountering moderate variations within groups, which allowed us to perform quantitative analysis. In the future, our experimental protocol will allow us to study a variety of restorative stroke treatments. We will use distinct stains to label different vascular structures in order to visualize neovascularization, venous vessels, microvessels and capillaries, tissues, cells and proteins, not only in case of stroke but also in additional pathologies. We can connect functional data with intricate macro and microstructures. In today's multidisciplinary environment, this will help us to identify treatments with clinical potential in ischemic stroke.

SUMMARY

To elucidate the process of microvasculature remodeling after ischemic stroke, a thorough analysis of the cerebral microvessels was performed. The tMCAO (transient middle cerebral artery occlusion)-mouse model proved suitable for the induction of local infarcts in the striatum and cortex. The optimized solvent-based clearing method provided an adequate basis for the analysis of the mouse brain microvasculature with Lichtblatt-Fluoreszenzmikroskopie (LSFM). Labeling of the mouse brain vasculature with hydrogel and FITC (fluorescein isothiocyanate)-conjugated albumin via cardiac perfusion allowed the visualization of the vascular structure with LSFM, enabling the detailed analysis of the vascular system. 3D (three dimension)-reconstruction and vascular quantification of healthy and ischemic hemispheres were successfully performed by fitting the imaging data to a filament-tracing model, which allowed the calculation of different vascular parameters for both healthy and ischemic tissues. In addition, treatment with the S1P (sphing-1-phosphate) receptor modulator FTY720 (Fingolimod) reduced the secondary damage in the infarct area, especially at 14 days following the stroke. Specifically, FTY720 treatment significantly increased microvascular density and branching point density in the infarct striatum after mild and after severe stroke and decreased infarct volume compared to vehicle treatment, suggesting in utility as restoration stroke treatment.

ZUSAMMENFASSUNG

Um den Umbau der Mikrogefäße nach einem ischämischen Schlaganfall zu verstehen, haben wir eine detaillierte Analyse der zerebralen Mikrogefäße durchgeführt. Das tMCAO (transient middle cerebral artery occlusion)-Model erwies sich als geeignetes Mausmodel, um lokale Infarkte in den Hirnhemisphären und der Hirnrinde zu induzieren. Das optimierte Lösungsmittel-Clearing-Verfahren lieferte eine adäquate Bildgebungsgrundlage für die Analyse der Mikrogefäße des Mäusegehirns mit Hilfe der Lichtblatt-Fluoreszenzmikroskopie (LSFM). Die Markierung der Hirngefäße der Maus mit Hydrogel und FITC (fluorescein isothiocyanate) konjugiertem Albumin über die Herzperfusion ermöglichte eine klare Darstellung der Gefäßstruktur im LSFM, wodurch eine detaillierte Analyse des Gefäßsystems möglich wurde. Die 3D (three dimension)-Rekonstruktion und vaskuläre Quantifizierung gesunder und ischämischer Hemisphären wurde erfolgreich durchgeführt, indem die Bildgebungsdaten an das Filamentmodel angepasst wurden, was die Berechnung verschiedener vaskulärer Daten sowohl für gesundes als auch für ischämisches Gewebe ermöglichte. Darüber hinaus reduzierte die Behandlung mit dem S1P (sphing-1-phosphate) Receptor Modulator FTY720 (Fingolimod) über einen Zeitraum von 14 Tagen den Sekundärschäden im Infarktgebiet. Insbesondere verbesserte die Behandlung mit FTY720 die Gefäß- und Verzweigungspunkt-Dichte im Striatum, sowohl nach einem leichten als auch nach einem schweren Schlaganfall, und verringerte das Infarktvolumen im Vergleich zu Trägestoff Behandlung, was auf eine restaurative Wirkung bei der Behandlung des Schlaganfalls schließen lässt.

REFERENCES

1. Allinson, K. R., Lee, H. S., Fruttiger, M., Mccarty, J. & Arthur, H. M. 2012. Endothelial expression of TGFβ type II receptor is required to maintain vascular integrity during postnatal development of the central nervous system. *PloS one,* 7**,** e39336.
2. Beck, H., Acker, T., Wiessner, C., Allegrini, P. R. & Plate, K. H. 2000. Expression of angiopoietin-1, angiopoietin-2, and tie receptors after middle cerebral artery occlusion in the rat. *The American journal of pathology,* 157**,** 1473-1483.
3. Benjamin, E. J., Muntner, P., Alonso, A., Bittencourt, M. S., Callaway, C. W., Carson, A. P., Chamberlain, A. M., Chang, A. R., Cheng, S. & Das, S. R. 2019. Heart disease and stroke statistics—2019 update: a report from the American Heart Association. *Circulation,* 139**,** e56-e528.
4. Billich, A., Bornancin, F., Dévay, P., Mechtcheriakova, D., Urtz, N. & Baumruker, T. 2003. Phosphorylation of the immunomodulatory drug FTY720 by sphingosine kinases. *Journal of Biological Chemistry,* 278**,** 47408-47415.
5. Blondeau, N., Lai, Y., Tyndall, S., Popolo, M., Topalkara, K., Pru, J. K., Zhang, L., Kim, H., Liao, J. K. & Ding, K. 2007. Distribution of sphingosine kinase activity and mRNA in rodent brain. *Journal of neurochemistry,* 103**,** 509-517.
6. Boero, J. A., Ascher, J., Arregui, A., Rovainen, C. & Woolsey, T. A. 1999. Increased brain capillaries in chronic hypoxia. *Journal of applied physiology,* 86**,** 1211-1219.
7. Brait, V. H., Tarrasón, G., Gavaldà, A., Godessart, N. & Planas, A. M. 2016. Selective sphingosine 1-phosphate receptor 1 agonist is protective against ischemia/reperfusion in mice. *Stroke,* 47**,** 3053-3056.
8. Brown, W. R. & Thore, C. R. 2011. Cerebral microvascular pathology in ageing and neurodegeneration. *Neuropathology and applied neurobiology,* 37**,** 56-74.
9. Chiba, K., Yanagawa, Y., Masubuchi, Y., Kataoka, H., Kawaguchi, T., Ohtsuki, M. & Hoshino, Y. 1998. FTY720, a novel immunosuppressant, induces sequestration of circulating mature lymphocytes by acceleration of lymphocyte homing in rats. I. FTY720 selectively decreases the number of circulating mature

lymphocytes by acceleration of lymphocyte homing. *The Journal of Immunology,* 160**,** 5037-5044.

10. Ciurică, S., Lopez-Sublet, M., Loeys, B. L., Radhouani, I., Natarajan, N., Vikkula, M., Maas, A. H., Adlam, D. & Persu, A. 2019. Arterial tortuosity: Novel implications for an old phenotype. *Hypertension,* 73**,** 951-960.
11. Conchello, J.-A. & Lichtman, J. W. 2005. Optical sectioning microscopy. *Nature methods,* 2**,** 920-931.
12. Corliss, B. A., Mathews, C., Doty, R., Rohde, G. & Peirce, S. M. 2019. Methods to label, image, and analyze the complex structural architectures of microvascular networks. *Microcirculation,* 26**,** e12520.
13. Ertürk, A., Becker, K., Jährling, N., Mauch, C. P., Hojer, C. D., Egen, J. G., Hellal, F., Bradke, F., Sheng, M. & Dodt, H.-U. 2012. Three-dimensional imaging of solvent-cleared organs using 3DISCO. *Nature protocols,* 7**,** 1983.
14. Fujii, M., Hara, H., Meng, W., Vonsattel, J. P., Huang, Z. & Moskowitz, M. A. 1997. Strain-related differences in susceptibility to transient forebrain ischemia in SV-129 and C57black/6 mice. *Stroke,* 28**,** 1805-1811.
15. Garcia, J. H., Liu, K.-F. & Ho, K.-L. 1995. Neuronal necrosis after middle cerebral artery occlusion in Wistar rats progresses at different time intervals in the caudoputamen and the cortex. *Stroke,* 26**,** 636-643.
16. Gautam, P., Anstey, K. J., Wen, W., Sachdev, P. S. & Cherbuin, N. 2015. Cortical gyrification and its relationships with cortical volume, cortical thickness, and cognitive performance in healthy mid-life adults. *Behavioural brain research,* 287**,** 331-339.
17. Green, A. R. & Shuaib, A. 2006. Therapeutic strategies for the treatment of stroke. *Drug discovery today,* 11**,** 681-693.
18. Group, N. R.-P. S. S. 2000. Effect of intravenous recombinant tissue plasminogen activator on ischemic stroke lesion size measured by computed tomography. *Stroke,* 31**,** 2912-2919.
19. Hacke, W., Kaste, M., Bluhmki, E., Brozman, M., Dávalos, A., Guidetti, D., Larrue, V., Lees, K. R., Medeghri, Z. & Machnig, T. 2008. Thrombolysis with alteplase 3 to 4.5 hours after acute ischemic stroke. *New England journal of medicine,* 359**,** 1317-1329.

20. Han, H.-C. 2012. Twisted blood vessels: symptoms, etiology and biomechanical mechanisms. *Journal of vascular research,* 49**,** 185-197.
21. Hassler, O. 1967. Arterial deformities in senile brains. *Acta neuropathologica,* 8**,** 219-229.
22. Hayashi, T., Noshita, N., Sugawara, T. & Chan, P. H. 2003. Temporal profile of angiogenesis and expression of related genes in the brain after ischemia. *J Cereb Blood Flow Metab,* 23**,** 166-80.
23. Hermann, D. M. & Chopp, M. 2012. Promoting brain remodelling and plasticity for stroke recovery: therapeutic promise and potential pitfalls of clinical translation. *The Lancet Neurology,* 11**,** 369-380.
24. Iwasawa, E., Ishibashi, S., Suzuki, M., Li, F., Ichijo, M., Miki, K. & Yokota, T. 2018. Sphingosine-1-phosphate receptor 1 activation enhances leptomeningeal collateral development and improves outcome after stroke in mice. *Journal of Stroke and Cerebrovascular Diseases,* 27**,** 1237-1251.
25. Jing, D., Zhang, S., Luo, W., Gao, X., Men, Y., Ma, C., Liu, X., Yi, Y., Bugde, A. & Zhou, B. O. 2018. Tissue clearing of both hard and soft tissue organs with the PEGASOS method. *Cell research,* 28**,** 803-818.
26. Johnson, W., Onuma, O., Owolabi, M. & Sachdev, S. 2016. Stroke: a global response is needed. *Bulletin of the World Health Organization,* 94**,** 634.
27. Kanazawa, M., Miura, M., Toriyabe, M., Koyama, M., Hatakeyama, M., Ishikawa, M., Nakajima, T., Onodera, O., Takahashi, T. & Nishizawa, M. 2017. Microglia preconditioned by oxygen-glucose deprivation promote functional recovery in ischemic rats. *Scientific reports,* 7**,** 1-16.
28. Kang, D.-W., Chu, K., Yoon, B.-W., Song, I. C., Chang, K.-H. & Roh, J.-K. 2000. Diffusion-weighted imaging in Wallerian degeneration. *Journal of the neurological sciences,* 178**,** 167-169.
29. Katan, M. & Luft, A. Global burden of stroke. Seminars in neurology, 2018. Thieme Medical Publishers, 208-211.
30. Keller, P. J. & Dodt, H.-U. 2012. Light sheet microscopy of living or cleared specimens. *Current opinion in neurobiology,* 22**,** 138-143.

31. Kiessling, F., Razansky, D. & Alves, F. 2010. Anatomical and microstructural imaging of angiogenesis. *European journal of nuclear medicine and molecular imaging,* 37**,** 4-19.

32. Koizumi, J. 1986. Experimental studies of ischemic brain edema. 1. A new experimental model of cerebral embolism in rats in which recirculation can be introduced in the ischemic area. *Jpn J stroke,* 8**,** 1-8.

33. Kraemer, M., Schormann, T., Hagemann, G., Qi, B., Witte, O. W. & Seitz, R. J. 2004. Delayed shrinkage of the brain after ischemic stroke: preliminary observations with voxel‐guided morphometry. *Journal of neuroimaging,* 14**,** 265-272.

34. Kraft, P., Göb, E., Schuhmann, M. K., Göbel, K., Deppermann, C., Thielmann, I., Herrmann, A. M., Lorenz, K., Brede, M. & Stoll, G. 2013. FTY720 ameliorates acute ischemic stroke in mice by reducing thrombo-inflammation but not by direct neuroprotection. *Stroke,* 44**,** 3202-3210.

35. Kuriakose, D. & Xiao, Z. 2020. Pathophysiology and treatment of stroke: present status and future perspectives. *International journal of molecular sciences,* 21**,** 7609.

36. Lai, H. M., Liu, A. K. L., Ng, H. H. M., Goldfinger, M. H., Chau, T. W., Defelice, J., Tilley, B. S., Wong, W. M., Wu, W. & Gentleman, S. M. 2018. Next generation histology methods for three-dimensional imaging of fresh and archival human brain tissues. *Nature communications,* 9**,** 1-12.

37. Lambertsen, K. L., Finsen, B. & Clausen, B. H. 2019. Post-stroke inflammation—target or tool for therapy? *Acta neuropathologica,* 137**,** 693-714.

38. Lambertsen, K. L., Gregersen, R., Meldgaard, M., Clausen, B. H., Heibøl, E. K., Ladeby, R., Knudsen, J., Frandsen, A., Owens, T. & Finsen, B. 2004. A role for interferon-gamma in focal cerebral ischemia in mice. *Journal of Neuropathology & Experimental Neurology,* 63**,** 942-955.

39. Liesz, A., Sun, L., Zhou, W., Schwarting, S., Mracsko, E., Zorn, M., Bauer, H., Sommer, C. & Veltkamp, R. 2011. FTY720 reduces post-ischemic brain lymphocyte influx but does not improve outcome in permanent murine cerebral ischemia. *PloS one,* 6**,** e21312.

40. Lin, C.-Y., Chang, C., Cheung, W.-M., Lin, M.-H., Chen, J.-J., Hsu, C. Y., Chen, J.-H. & Lin, T.-N. 2008. Dynamic changes in vascular permeability, cerebral blood volume, vascular density, and size after transient focal cerebral ischemia in rats: evaluation with contrast-enhanced magnetic resonance imaging. *Journal of Cerebral Blood Flow & Metabolism,* 28**,** 1491-1501.
41. Lin, T.-N., He, Y. Y., Wu, G., Khan, M. & Hsu, C. Y. 1993. Effect of brain edema on infarct volume in a focal cerebral ischemia model in rats. *Stroke,* 24**,** 117-121.
42. Liu, J., Wang, Y., Akamatsu, Y., Lee, C. C., Stetler, R. A., Lawton, M. T. & Yang, G.-Y. 2014. Vascular remodeling after ischemic stroke: mechanisms and therapeutic potentials. *Progress in neurobiology,* 115**,** 138-156.
43. Lugo-Hernandez, E., Squire, A., Hagemann, N., Brenzel, A., Sardari, M., Schlechter, J., Sanchez-Mendoza, E. H., Gunzer, M., Faissner, A. & Hermann, D. M. 2017. 3D visualization and quantification of microvessels in the whole ischemic mouse brain using solvent-based clearing and light sheet microscopy. *Journal of Cerebral Blood Flow & Metabolism,* 37**,** 3355-3367.
44. Malone, K., Diaz Diaz, A. C., Shearer, J. A., Moore, A. C. & Waeber, C. 2021. The effect of fingolimod on regulatory T cells in a mouse model of brain ischaemia. *Journal of neuroinflammation,* 18**,** 1-15.
45. Manoonkitiwongsa, P. S., Jackson-Friedman, C., Mcmillan, P. J., Schultz, R. L. & Lyden, P. D. 2001. Angiogenesis after stroke is correlated with increased numbers of macrophages: the clean-up hypothesis. *Journal of Cerebral Blood Flow & Metabolism,* 21**,** 1223-1231.
46. Marti, H. J., Bernaudin, M., Bellail, A., Schoch, H., Euler, M., Petit, E. & Risau, W. 2000. Hypoxia-induced vascular endothelial growth factor expression precedes neovascularization after cerebral ischemia. *The American journal of pathology,* 156**,** 965-976.
47. Mcdonald, D. M. & Choyke, P. L. 2003. Imaging of angiogenesis: from microscope to clinic. *Nature medicine,* 9**,** 713-725.
48. Menon, B., Smith, E., Modi, J., Patel, S., Bhatia, R., Watson, T., Hill, M., Demchuk, A. & Goyal, M. 2011. Regional leptomeningeal score on CT angiography predicts clinical and imaging outcomes in patients with acute anterior circulation occlusions. *American journal of neuroradiology,* 32**,** 1640-1645.

49. Merz, S. F., Korste, S., Bornemann, L., Michel, L., Stock, P., Squire, A., Soun, C., Engel, D. R., Detzer, J. & Lörchner, H. 2019. Contemporaneous 3D characterization of acute and chronic myocardial I/R injury and response. *Nature communications,* 10**,** 1-14.

50. Miteff, F., Levi, C. R., Bateman, G. A., Spratt, N., Mcelduff, P. & Parsons, M. W. 2009. The independent predictive utility of computed tomography angiographic collateral status in acute ischaemic stroke. *Brain,* 132**,** 2231-2238.

51. Mohamud Yusuf, A., Hagemann, N., Schulten, S., Rausch, O., Wagner, K., Hussner, T., Qi, Y., Totzeck, M., Kleinschnitz, C. & Squire, A. 2021. Light Sheet Microscopy Using FITC-Albumin Followed by Immunohistochemistry of the Same Rehydrated Brains Reveals Ischemic Brain Injury and Early Microvascular Remodeling. *Frontiers in Cellular Neuroscience***,** 459.

52. Müller, T., Haraldseth, O. & Unsgård, G. 1994. Characterization of the microcirculation during ischemia and reperfusion in the penumbra of a rat model of temporary middle cerebral artery occlusion: a laser Doppler flowmetry study. *International Journal of Microcirculation,* 14**,** 289-295.

53. Murphy, S. J. & Werring, D. J. 2020. Stroke: causes and clinical features. *Medicine*.

54. Naseh, M., Vatanparast, J., Rafati, A., Bayat, M. & Haghani, M. 2021. The emerging role of FTY720 as a sphingosine 1‐phosphate analog for the treatment of ischemic stroke: The cellular and molecular mechanisms. *Brain and Behavior***,** e02179.

55. Nogueira, R. G., Lutsep, H. L., Gupta, R., Jovin, T. G., Albers, G. W., Walker, G. A., Liebeskind, D. S. & Smith, W. S. 2012. Trevo versus Merci retrievers for thrombectomy revascularisation of large vessel occlusions in acute ischaemic stroke (TREVO 2): a randomised trial. *The Lancet,* 380**,** 1231-1240.

56. Pampaloni, F., Chang, B.-J. & Stelzer, E. H. 2015. Light sheet-based fluorescence microscopy (LSFM) for the quantitative imaging of cells and tissues. *Cell and tissue research,* 360**,** 129-141.

57. Pantoni, L. 2010. Cerebral small vessel disease: from pathogenesis and clinical characteristics to therapeutic challenges. *The Lancet Neurology,* 9**,** 689-701.

58. Pardridge, W. M. 1999. Blood-brain barrier biology and methodology. *Journal of neurovirology,* 5**,** 556-569.

59. Pardridge, W. M. 2001. Brain drug targeting and gene technologies. *The Japanese journal of pharmacology,* 87**,** 97-103.

60. Pascu, A., Romanitan, M. O., Delgado, J. M., Danaila, L. & Pascu, M. L. 2009. Laser - Induced Autofluorescence Measurements on Brain Tissues. *The Anatomical Record: Advances in Integrative Anatomy and Evolutionary Biology: Advances in Integrative Anatomy and Evolutionary Biology,* 292**,** 2013-2022.

61. Paugh, S. W., Payne, S. G., Barbour, S. E., Milstien, S. & Spiegel, S. 2003. The immunosuppressant FTY720 is phosphorylated by sphingosine kinase type 2. *FEBS letters,* 554**,** 189-193.

62. Pinschewer, D. D., Ochsenbein, A. F., Odermatt, B., Brinkmann, V., Hengartner, H. & Zinkernagel, R. M. 2000. FTY720 immunosuppression impairs effector T cell peripheral homing without affecting induction, expansion, and memory. *The Journal of Immunology,* 164**,** 5761-5770.

63. Popa-Wagner, A., Pirici, D., Bogdan Petcu, E., Mogoanta, L., Buga, A.-M., L Rosen, C., Leon, R. & D Huber, J. 2010. Pathophysiology of the vascular wall and its relevance for cerebrovascular disorders in aged rodents. *Current neurovascular research,* 7**,** 251-267.

64. Prabhakaran, S., Ruff, I. & Bernstein, R. A. 2015. Acute stroke intervention: a systematic review. *Jama,* 313**,** 1451-1462.

65. Qi, Y., Yu, T., Xu, J., Wan, P., Ma, Y., Zhu, J., Li, Y., Gong, H., Luo, Q. & Zhu, D. 2019. FDISCO: Advanced solvent-based clearing method for imaging whole organs. *Science advances,* 5**,** eaau8355.

66. Richardson, D. S. & Lichtman, J. W. 2015. Clarifying tissue clearing. *Cell,* 162**,** 246-257.

67. Rodrigo, R., Fernández-Gajardo, R., Gutiérrez, R., Manuel Matamala, J., Carrasco, R., Miranda-Merchak, A. & Feuerhake, W. 2013. Oxidative stress and pathophysiology of ischemic stroke: novel therapeutic opportunities. *CNS & Neurological Disorders-Drug Targets (Formerly Current Drug Targets-CNS & Neurological Disorders),* 12**,** 698-714.

68. Salas-Perdomo, A., Miró-Mur, F., Gallizioli, M., Brait, V. H., Justicia, C., Meissner, A., Urra, X., Chamorro, A. & Planas, A. M. 2019. Role of the S1P pathway and inhibition by fingolimod in preventing hemorrhagic transformation after stroke. *Scientific reports,* 9**,** 1-13.

69. Santi, P. A. 2011. Light sheet fluorescence microscopy: a review. *Journal of Histochemistry & Cytochemistry,* 59**,** 129-138.

70. Saver, J. L., Jahan, R., Levy, E. I., Jovin, T. G., Baxter, B., Nogueira, R. G., Clark, W., Budzik, R. & Zaidat, O. O. 2012. Solitaire flow restoration device versus the Merci Retriever in patients with acute ischaemic stroke (SWIFT): a randomised, parallel-group, non-inferiority trial. *The Lancet,* 380**,** 1241-1249.

71. Scholz, D., Cai, W.-J. & Schaper, W. 2001. Arteriogenesis, a new concept of vascular adaptation in occlusive disease. *Angiogenesis,* 4**,** 247-257.

72. Schroeter, M., Jander, S., Witte, O. W. & Stoll, G. 1994. Local immune responses in the rat cerebral cortex after middle cerebral artery occlusion. *Journal of neuroimmunology,* 55**,** 195-203.

73. Siedentopf, H. & Zsigmondy, R. 1902. Uber sichtbarmachung und größenbestimmung ultramikoskopischer teilchen, mit besonderer anwendung auf goldrubingläser. *Annalen der Physik,* 315**,** 1-39.

74. Sims, N. R. & Muyderman, H. 2010. Mitochondria, oxidative metabolism and cell death in stroke. *Biochimica et Biophysica Acta (BBA)-Molecular Basis of Disease,* 1802**,** 80-91.

75. Slevin, M., Kumar, P., Gaffney, J., Kumar, S. & Krupinski, J. 2006. Can angiogenesis be exploited to improve stroke outcome? Mechanisms and therapeutic potential. *Clinical Science,* 111**,** 171-183.

76. Smith, W. S., Sung, G., Saver, J., Budzik, R., Duckwiler, G., Liebeskind, D. S., Lutsep, H. L., Rymer, M. M., Higashida, R. T. & Starkman, S. 2008. Mechanical thrombectomy for acute ischemic stroke: final results of the Multi MERCI trial. *Stroke,* 39**,** 1205-1212.

77. Smith, W. S., Sung, G., Starkman, S., Saver, J. L., Kidwell, C. S., Gobin, Y. P., Lutsep, H. L., Nesbit, G. M., Grobelny, T. & Rymer, M. M. 2005. Safety and efficacy of mechanical embolectomy in acute ischemic stroke: results of the MERCI trial. *Stroke,* 36**,** 1432-1438.

78. Stelzer, E. H. 2015. Light-sheet fluorescence microscopy for quantitative biology. *Nature methods,* 12**,** 23-26.

79. Stoll, G. & Nieswandt, B. 2019. Thrombo-inflammation in acute ischaemic stroke — implications for treatment. *Nature Reviews Neurology,* 15**,** 473-481.

80. Susaki, E. A., Tainaka, K., Perrin, D., Kishino, F., Tawara, T., Watanabe, T. M., Yokoyama, C., Onoe, H., Eguchi, M. & Yamaguchi, S. 2014. Whole-brain imaging with single-cell resolution using chemical cocktails and computational analysis. *Cell,* 157**,** 726-739.

81. Tsai, P. S., Kaufhold, J. P., Blinder, P., Friedman, B., Drew, P. J., Karten, H. J., Lyden, P. D. & Kleinfeld, D. 2009. Correlations of neuronal and microvascular densities in murine cortex revealed by direct counting and colocalization of nuclei and vessels. *Journal of Neuroscience,* 29**,** 14553-14570.

82. Werring, D. J., Toosy, A. T., Clark, C. A., Parker, G. J., Barker, G. J., Miller, D. H. & Thompson, A. J. 2000. Diffusion tensor imaging can detect and quantify corticospinal tract degeneration after stroke. *Journal of Neurology, Neurosurgery & Psychiatry,* 69**,** 269-272.

83. Xiong, X., Barreto, G. E., Xu, L., Ouyang, Y. B., Xie, X. & Giffard, R. G. 2011. Increased brain injury and worsened neurological outcome in interleukin-4 knockout mice after transient focal cerebral ischemia. *Stroke,* 42**,** 2026-2032.

84. Xiong, Y., Mahmood, A. & Chopp, M. 2010. Angiogenesis, neurogenesis and brain recovery of function following injury. *Current opinion in investigational drugs (London, England: 2000),* 11**,** 298.

85. Yilmaz, G., Arumugam, T. V., Stokes, K. Y. & Granger, D. N. 2006. Role of T lymphocytes and interferon-γ in ischemic stroke. *Circulation,* 113**,** 2105-2112.

86. Yoshimura, A. & Shichita, T. 2012. Post-ischemic inflammation in the brain. *Frontiers in immunology,* 3**,** 132.

87. Yu, S. W., Friedman, B., Cheng, Q. & Lyden, P. D. 2007. Stroke-evoked angiogenesis results in a transient population of microvessels. *Journal of Cerebral Blood Flow & Metabolism,* 27**,** 755-763.

ATTACHMENT

1.25 List of abbreviations

ATP	Adenosine triphosphate
BBB	Blood-brain barrier
BP	Branching points
CBV	Cerebral blood volume
CD	Cluster of differentiation
CCA	Common carotid artery
DBE	Dibenzyl ether
ECi	Ethyl cinnamate
FDA	Food and Drug Administration
FDISCO	Fluorescent three-dimensional imaging of solvent-cleared organs
FTY720	Fingolimod
FITC	Fluorescein isothiocyanate
FoxP3+	Forkhead box P3
IB4	Isolectin B4
ICA	Internal carotid artery
IL	Interleukin
INF	Interferon
LDF	Laser Dopper flowmetry
LSFM	Light-sheet fluorescence microscopy
MCA	Middle cerebral artery
MRI	Magnetic resonance imaging
MS	Multiple sclerosis
N_2O	Nitrogen dioxide
O_2	Oxygen
PBS	Phosphate-buffered saline

PFA	Paraformaldehyde
RNs	Reactive nitrogen species
ROI	Region of interest
ROs	Reactive oxygen species
rt-PA	Recombinant tissue plasminogen activator
S1P	Sphingosine-1-phosphorate
3D	Three-dimensional
THF	Tetrahydrofuran
tMCAO	Transient middle cerebral artery occlusion
TNF	Tumor necrosis factor
TTC	Triphenyl tetrazolium chloride
VLD	Vessel-length density
VMTK	Vascular modeling toolkit

1.26 List of tables

1.27 List of figures

1.28 Statement of permission

This thesis is partly based on a manuscript in writing. The data of our collaborator, AG Gunzer of the University Hospital Essen and the Institute of Academic Imaging, are introduced here with their permission.

ACKNOWLEDGEMENTS

I would like to express my gratitude to the following people.

First of all, I am very grateful to my supervisor, Prof. Dirk Hermann, for making me a part of this laboratory, where there are colleagues and students from various countries, studying and working together, in which I experienced the satisfaction and difficulties of research, as well as the embracing and heartwarming nature of the team. I did not feel lonely in a foreign country, and I also learned many world-class skills and methods. In this pleasant atmosphere, I enjoyed spending my MD time.

I would like to thank Dr. rer. nat. Nina Hagemann for leading me into the interesting research field of 3D reconstruction and angiogenesis of cerebral blood vessels and for helping me with my thesis and other aspects. In addition, I would like to thank Dr. rer. nat. Anthony Squire, Universitätsklinikum Essen, Essen Imaging Center, kindly taught me a lot about microscopy, enabling me to use microscopy and computer software to complete my 3D reconstructions and to complete my data analysis.

I would further like to thank my colleagues Britta Kaltwasser, Maryam Sardari, Chen Wang, Dongpei Yin, Anran Li, Egor Dzyubenko, Tayana Silva de Carvalho, and Ayan Mohamud Yusuf, for their kindness and help in completing this high-level subject.

Additionally, I am very appreciative of my British friend Benjamin and my Alumni Enzo Ch'I Nio and Venkatesh Kumar Chetty who are at all time ready to help me with my English modification

Further, I would like to thank the China Scholarship Council for providing me with financial support so that I could complete my studies without worries.

Finally, I would like to express my gratitude to my family in China for their understanding and support.

Der Lebenslauf ist in der Online-Version aus Gründen des Datenschutzes nicht enthalten.